NASA TN D-1257

NASA TN D-1257

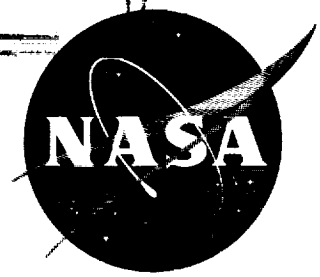

TECHNICAL NOTE

D-1257

DIVISION OF AERODYNAMIC LOADS ON A SEMISPAN TILTING-DUCTED-PROPELLER MODEL IN HOVERING AND TRANSITION FLIGHT

By Kalman J. Grunwald and Kenneth W. Goodson

Langley Research Center
Langley Station, Hampton, Va.

NATIONAL AERONAUTICS AND SPACE ADMINISTRATION
WASHINGTON May 1962

NATIONAL AERONAUTICS AND SPACE ADMINISTRATION

TECHNICAL NOTE D-1237

DIVISION OF AERODYNAMIC LOADS ON A SEMISPAN TILTING-DUCTED-PROPELLER MODEL IN HOVERING AND TRANSITION FLIGHT

By Kalman J. Grunwald and Kenneth W. Goodson

SUMMARY

An investigation to determine the division of aerodynamic loads on a wing-tip-mounted ducted-propeller configuration was conducted in the 17-foot test section of the Langley 300-MPH 7- by 10-foot tunnel. The semispan-model tests were conducted through a duct-angle range (90° to 0°) and an advance-ratio range (0 to 0.699) to cover conditions of hovering flight and transition flight.

Most of the normal-force and pitching-moment loads experienced by the configuration were carried by the duct at transition speeds. The propeller and wing contribution to the overall normal force and pitching moment were small.

The overall lift of the configuration can be increased through the transition speed range by flying at a positive angle of attack and by the addition of some high-lift device such as a flap.

INTRODUCTION

At the present time the tilt-duct aircraft is being considered as one of the possible desirable configurations for a propeller-driven VTOL aircraft. (See ref. 1.) The ducted propeller is favored for some applications because of the reduction in propeller diameter made possible by using the duct and because of the protection to personnel afforded by the duct. Some information on a ducted-propeller configuration is presented in references 2 to 5, including some data on the division of loads between the propeller and the duct in reference 3. The purpose of the present investigation was to determine the division of loads between the wing and duct on a wing-tip-mounted ducted-propeller configuration and to obtain additional data on the division of loads between the propeller and duct.

The present investigation was conducted with two duct inlet configurations. In hovering and low-speed flight a large (static) inlet was used. In the cruise condition such an inlet would have been undesirable because of its high drag. For this reason an inlet with a small leading-edge radius was provided for the high-speed flight condition. An aircraft based on this model would therefore be required to have an inlet with variable geometry.

The model testing was conducted in the 17-foot test section of the Langley 300-MPH 7- by 10-foot tunnel. Data are presented for a number of duct angles (90° to 0°) and advance ratios (0 to 0.699) through a wing angle-of-attack range. The duct angles and advance ratios were chosen to cover the flight conditions for hovering and transition. Data are also presented for the high-speed or cruise condition.

The effect of the ground and the effect of deflecting the slipstream by deflector vanes in the rear of the duct were also investigated.

SYMBOLS

A axial force, total configuration, lb

A_D axial force, duct-propeller combination, lb

A_P axial force, propeller, lb

b wing and duct span (60 in., twice the span of semispan model, used in nondimensionalizing data), in.

C_L lift coefficient, $\frac{L}{qS}$

C_{M_X} total semispan configuration bending-moment coefficient (X-axis) (see fig. 5), $\frac{M_X}{qS\frac{b}{2}}$

C_{M_Y} total configuration pitching-moment coefficient (see fig. 5), $\frac{M_Y}{qSc}$

C_{M_Z} total semispan configuration bending-moment coefficient (Z-axis) (see fig. 5), $\frac{M_Z}{qS\frac{b}{2}}$

C_P power coefficient, $\frac{2\pi nQ}{\rho n^3 d^5}$

C_T propeller thrust coefficient, $\frac{T_P}{\rho n^2 d^4}$

C_X longitudinal force coefficient, $\frac{X}{qS}$

c wing chord, 9.66 in.

d propeller diameter, 13.24 in.

d_D duct exit diameter, 14.03 in.

h distance from duct pivot to groundboard

L total configuration lift (based on full span), lb

l propeller moment transfer distance, 1.45 in.

M_X total semispan configuration bending moment (X-axis), including propeller torque component (see fig. 5), ft-lb

$M_{X,D}$ duct bending moment (X-axis), including propeller torque component (see fig. 5), ft-lb

M_Y total configuration pitching moment, ft-lb

$M_{Y,D}$ duct total pitching moment, including propeller moment, ft-lb

$M_{Y,P}$ propeller pitching moment, ft-lb

M_Z total semispan configuration bending moment (Z-axis), including propeller torque component (see fig. 5), ft-lb

$M_{Z,D}$ duct bending moment (Z-axis), including propeller torque component (see fig. 5), ft-lb

N total configuration normal force, lb

N_D duct normal force, including propeller normal force, lb

N_P propeller normal force, lb

n	propeller rotational speed, $133\frac{1}{3}$ rps
Q	propeller motor torque, ft-lb
q	dynamic pressure, $\frac{1}{2}\rho V^2$
r/R	ratio of the radius of the propeller blade element to the propeller-tip radius
S	total wing and duct planform area (total wing area, 292 in.), 534 sq in.
T_D	duct plus propeller thrust, lb
T_P	propeller thrust, lb
T_o	hovering thrust $\left(T_{D,\text{hovering}} = 60 \text{ lb, based on two-duct configuration}\right)$
V	free-stream velocity, ft/sec unless otherwise noted
X	longitudinal force (wind axes), lb
α	wing angle of attack, deg
β	blade-section angle, 24° measured at the 75-percent blade span, deg
δ	duct deflection, measured from the wing chord line (see fig. 5), deg
ρ	density, slugs/cu ft

MODEL DESCRIPTION

Photographs showing two views of the model mounted in the tunnel are presented in figure 1. A two-view drawing of the model is shown in figure 2.

The model was mounted on a reflection plane 3 feet above the floor of the tunnel in order to have the model located in a more uniform flow field. The wing of the model was constructed of wood. A steel spar ran through the center of the wing to support the duct. The semispan wing was mounted on a five-component strain-gage balance.

The duct loads were measured on a six-component strain-gage balance which attached the duct to the wing. This balance slipped into a clamp arrangement inside the wing, so that the duct could be rotated through 360° and set at any desired incidence with respect to the wing. The total propeller and spinner forces were measured by strain-gage beams inside the motor nacelle housing.

Figure 2 shows the two duct inlets used during the tests. The geometric characteristics of the duct are presented in figure 3. The lines of the static inlet were generated by deflecting the forward 17 percent of the duct chord outward 45° as shown in figure 2.

The six-blade propeller was constructed of glass fiber with a plastic filler. Propeller-blade characteristics are presented in figure 4. For all the power-on tests the propeller blade angle was set at 24° at the 75-percent blade radius and the propeller rotational speed was 8,000 rpm. The propeller blades had a tip clearance of 0.1 inch.

A few tests were run with steel deflector vanes in the rear of the model as shown in figures 1 and 2. A split flap (fig. 2) was also used for some of the tests.

Ground-effect tests were conducted with an 8- by 8-foot groundboard located 17.89 inches from the duct pivot. The groundboard extended 3 feet ahead of and 5 feet behind the balance center line.

TEST TECHNIQUE

The test conditions were chosen to simulate flight transitions for zero longitudinal force at wing angles of attack of 0° and 10°. The condition of zero longitudinal force will correspond to steady level flight when the data are scaled so that the lift equals any assumed airplane weight at the angles of attack for zero longitudinal force. The scaling parameters presented in reference 2 can be used for this purpose. The data, as presented, are not conditions of steady level flight because the lift is not constant; however, the zero longitudinal force condition will be referred to as a steady level flight condition throughout this paper for convenience.

The test procedure consisted of setting the propeller rotational speed at 8,000 rpm, with the model wing at angles of attack of 0° or 10° for a given duct angle, then adjusting the tunnel speed until zero longitudinal force on the model was obtained. This tunnel speed produced the advance ratio required for a condition of steady level flight at wing angles of attack of 0° or 10° (depending on the desired angle of attack for zero longitudinal force). This speed was held constant as the data

were taken through an angle-of-attack range. A similar procedure was used to obtain simulated accelerating and decelerating flight conditions by testing at tunnel speeds above and below the speed for steady level flight.

The power-off Reynolds number was about 500,000 based on a wing chord of 9.66 inches. The maximum tunnel velocity was approximately 100 feet per second.

No wind-tunnel corrections have been applied to the data; however, corrections are believed to be small. For possible insight into tunnel-wall corrections reference 6 can be used.

PRESENTATION OF RESULTS

The free-stream dynamic pressure was used to nondimensionalize the power-off data and some power-on data in the relatively high-speed flight condition. However, in the transition speed range, coefficient data based on the free-stream velocity would approach infinite values near hovering flight. To avoid this problem transition-speed-range data have been nondimensionalized by dividing by the hovering thrust. This thrust (60 pounds) used to nondimensionalize the data was obtained from the hovering condition in the tunnel ($\delta = 90^\circ$, $\alpha \approx 0^\circ$). Data in figures 6 to 20 have been nondimensionalized based on this hovering thrust. Velocity has been nondimensionalized by using V/nd. The value of nd was held constant at 147 feet per second throughout the tests. Figure 21 presents coefficients based on the free-stream dynamic pressure.

Positive sense of forces, moments, and angles is presented in figure 5. Moment reference points are indicated in figures 2 and 5.

The basic division-of-loads data (figs. 6 to 16) are presented about different reference axes. Pictured with each set of data is the appropriate axis system about which that set of data has been presented.

The experimental results of this investigation are shown in the following figures:

DISCUSSION AND ANALYSIS

Division of Loads

Pitching moment and normal force.- The primary purpose of this investigation was to determine the division of loads on a wing-tip-mounted duct. The data in figures 6, 7, 8, and 9 represent typical advance ratios and duct angles for a steady-level-flight transition from hovering to forward flight. The data in figures 6 and 7 represent a steady level flight condition with α near 0°; figures 8 and 9 show corresponding data for a steady level flight condition with α near 10°. A comparison of the data in figures 6(b) and 6(c) shows that the normal force and pitching moment of the duct-propeller combination is essentially equal to the normal force and pitching moment of the entire configuration.

Figure 6(d) presents the forces and pitching moments of the duct-propeller combination referred to the duct body axes. Figure 6(e) is a plot of the propeller forces and pitching moments presented about the

duct body axes. It can be seen in figure 6(d) and figure 6(e) as well as in the remaining basic figures 7 to 16 (parts (d) and (e)) that most of the normal force and pitching moment is being carried on the duct. These data are in agreement with the results of reference 3 in which a ducted-propeller arrangement (without a wing) showed that most of the normal force and pitching-moment load was on the duct. Figure 19, which is based on data taken from figures 6, 7, 8, and 9, indicates more clearly the division of pitching moment between all components of the configuration.

Thrust and axial force.- In parts (d) and (e) of figures 6 to 16 the division of loads between the propeller axial force (thrust) and the total-duct axial force is presented. In figure 17 a comparison of propeller thrust to total thrust has been presented for a number of advance ratios through an angle-of-attack range. For the static inlet at the lower advance ratios and higher angles of attack T_P/T_D remains nearly constant. However, as advance ratio is increased and angle of attack decreased T_P/T_D increases rapidly. This increase is due to flow separation from the external surface of the static inlet. The cruise inlet, which does not experience external lip stall at the advance ratios shown, experiences only a small increase in T_P/T_D with decreasing angle of attack. At the advance ratios of the tests the cruise inlet is still carrying the same percentage of the thrust that it carried statically. The reason for the higher value of T_P/T_D for the configuration with the cruise inlet than for the configuration with the static inlet in hovering $\left(\text{fig. } 17(b);\ \alpha + \delta = 90^\circ;\ \frac{V}{nd} = 0\right)$ appears to be an internal flow separation near the leading edge of the cruise inlet configuration which decreases the duct thrust.

Two typical transitions which correspond to a steady level flight condition $\left(\alpha_{(X=0)} \approx 0^\circ,\ \alpha_{(X=0)} \approx 10^\circ\right)$ have been presented in figure 18 as a function of advance ratio. In hovering (V/nd = 0) approximately 50 percent of the total thrust is coming from the static inlet duct. As the speed is increased (V/nd = 0.7) the large increase in drag due to flow separation (as previously mentioned) causes T_P/T_D to rise sharply.

For the cruise inlet duct in hovering the ratio of T_P/T_D is 0.6 as compared with 0.5 for the static inlet duct at $\alpha \approx 10^\circ$. Internal lip stall on the cruise inlet duct causes duct thrust to decrease; therefore, a higher ratio of T_P/T_D results. Advance ratios representative of true cruising flight were not covered in the investigation, but other data (ref. 7) indicate that at cruising conditions the duct contribution to thrust is very small and can be slightly negative.

L
1
9
0
0

Wing and flap effectiveness.- In figures 20(a) and (b) lift data have been presented as a function of advance ratio for two typical steady level flight transitions ($\alpha_{(X=0)} \approx 0^\circ$ and $\alpha_{(X=0)} \approx 10^\circ$). Transition-speed-range data for a split flap deflected 50° is also presented. The main purpose of this plot is to indicate the effectiveness of the wing and a flap in carrying the lift load in the transition.

It can be seen from figure 20(a) that in a transition at an angle of attack of 0° essentially all the lift is carried on the duct-propeller combinations. By increasing angle of attack and deflecting a flap (fig. 20(b)) the wing contribution to lift can be appreciably increased, but within the range of this investigation the duct is still carrying most of the load. As previously noted, the propeller carries half the load in hovering and at very low speeds.

Ground effect.- Basic division-of-loads data are presented for a ground-effect condition ($h/c = 1.85$) in figures 14 and 15. Figure 20(c) is a comparison of the division of lift loads through the transition speed range for the configuration in ground effect with those for the configuration out of ground effect. No noticeable difference for the division of loads or for the overall loads is evident between the data for the configurations in and out of ground effect.

Other data presented.- Model power coefficient, thrust coefficient, and propeller pitching moment are presented in part (f) of figures 6 to 16. Bending moments of both the entire configuration and the duct only are presented in parts (g) and (h) of figures 6 to 16.

Division-of-loads data are also presented for the static duct configuration with deflector vanes in the rear of the duct (fig. 16). The purpose of the deflector vanes was to deflect the duct slipstream to the sides of the model. Similar vanes might be used in the hovering configuration of an aircraft when the duct slipstream would interfere with any operations being conducted directly beneath.

Flight Characteristics

Cruise configuration.- The power-off and high-speed power-on data are presented in figure 21. The high drag of the static inlet configuration is due to flow separations from the back of the static inlet as previously mentioned.

The power-on data plots for the wing and the static duct of figure 21 indicate a break in the lift—longitudinal-force polar near a lift

coefficient of 1.4. This break is due to the wing stall as indicated by the data in figure 9, parts (b) and (c) ($V/nd = 0.689$, $\delta = 0^\circ$). The normal force of the total configuration (fig. 9(b)) indicates a break in the curve at an angle of attack of approximately 20°. The normal-force plots of the duct (fig. 9(c)) show no change in the slope of the curve up to an angle of attack of 30°; therefore, with no indication of slope change on the duct it can be concluded that the duct is not stalled.

Transition performance.- A direct comparison of the transition flight characteristics of the configuration in the present paper has been made with the configuration of reference 2 in figure 22. The assumed aircraft weighs 3,000 pounds, as in reference 2, and has an exit diameter of 54.05 inches; in this manner the same exit area loading is maintained.

The power required in the present investigation appears to be somewhat higher than that of reference 2. A possible reason for the higher power required is the larger tip clearance of the propellers in the present investigation (0.1 inch as compared with 0.04 inch for ref. 2). References 8 and 9, reports which discuss tip clearance effects, give further insight into possible thrust and power losses. The different propeller geometry in the present investigation may also contribute to the higher power.

The smaller pitching moments experienced on the present model are probably due to the shorter distance from the inlet to the moment reference point.

CONCLUDING REMARKS

As the result of an investigation of the division of aerodynamic loads on a wing-tip-mounted ducted-propeller model, the following general conclusions have been observed:

1. The duct is the primary source of the total-configuration normal force and pitching moment in the transition speed range.

2. In hovering, for the static duct configuration approximately 50 percent of the total thrust is produced by the duct and 50 percent is produced by the propeller.

3. The overall lift of the configuration can be increased through the transition speed range by flying at a positive angle of attack and by the addition of some high-lift device such as a flap.

Langley Research Center,
National Aeronautics and Space Administration,
Langley Air Force Base, Va., February 19, 1961.

REFERENCES

1. Kuhn, Richard E.: Review of Basic Principles of V/STOL Aerodynamics. NASA TN D-733, 1961.

2. Goodson, Kenneth W., and Grunwald, Kalman J.: Aerodynamic Characteristics of a Powered Semispan Tilting-Shrouded-Propeller VTOL Model in Hovering and Transition Flight. NASA TN D-981, 1962.

3. Grunwald, Kalman J., and Goodson, Kenneth W.: Aerodynamic Loads of an Isolated Shrouded-Propeller Configuration for Angles of Attack From -10° to 110°. NASA TN D-995, 1962.

4. Yaggy, Paul F., and Goodson, Kenneth W.: Aerodynamics of a Tilting Ducted Fan Configuration. NASA TN D-785, 1961.

5. Yaggy, Paul F., and Mort, Kenneth W.: A Wind-Tunnel Investigation of a 4-Foot-Diameter Ducted Fan Mounted on the Tip of a Semispan Wing. NASA TN D-776, 1961.

6. Heyson, Harry H.: Linearized Theory of Wind-Tunnel Jet-Boundary Corrections and Ground Effect for VTOL-STOL Aircraft. NASA TR R-124, 1962.

7. Grose, Ronald M.: Wind-Tunnel Tests of Shrouded Propellers at Mach Numbers From 0 to 0.60. WADC Tech. Rep. 58-604, ASTIA Doc. No. AD-205464, U.S. Air Force, Dec. 1958.

8. Hoehne, Vernon O., and Hoffman, Hans: Shrouded Propeller Investigations: Propeller Tip Clearance Effects. Eng. Rep. No. 213-15 (Contract NONR 201(01)), Univ. of Wichita, Apr. 1961.

9. Hubbard, Harvey H.: Sound Measurements for Five Shrouded Propellers at Static Conditions. NACA TN 2024, 1950.

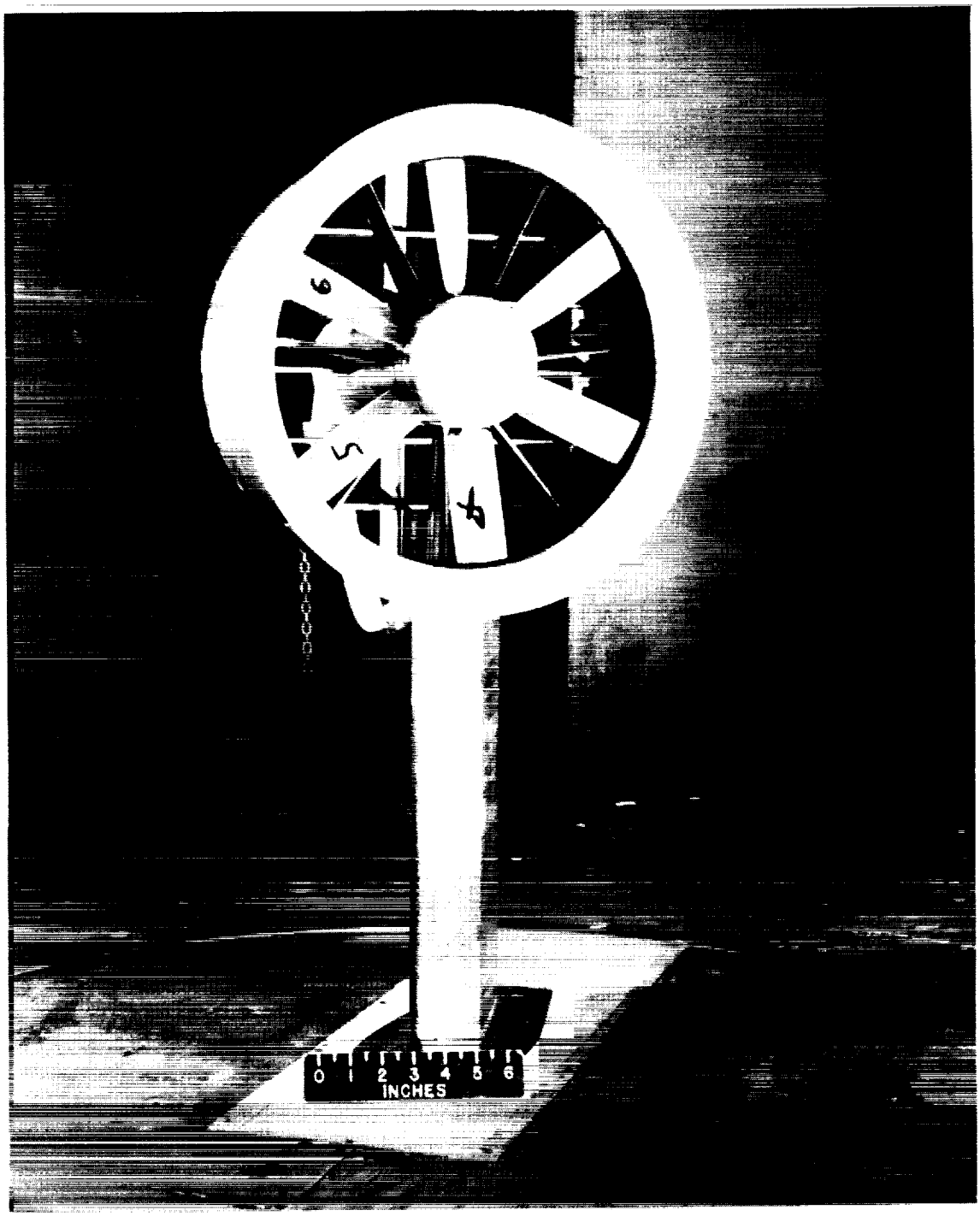

(a) Front view.

Figure 1.- Photographs of model in tunnel. L-61-1366

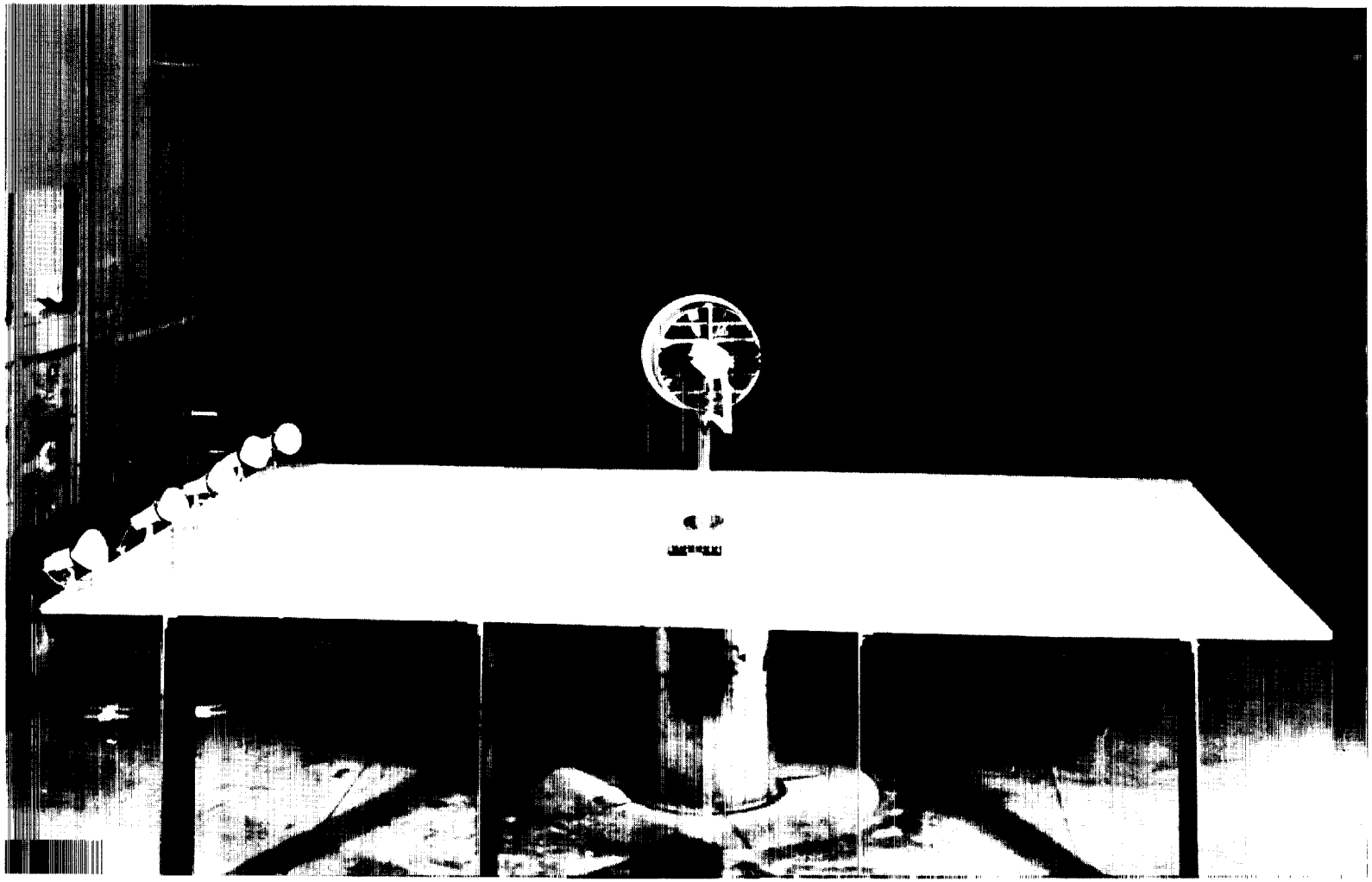

(b) Rear view.

Figure 1.- Concluded. L-61-1365

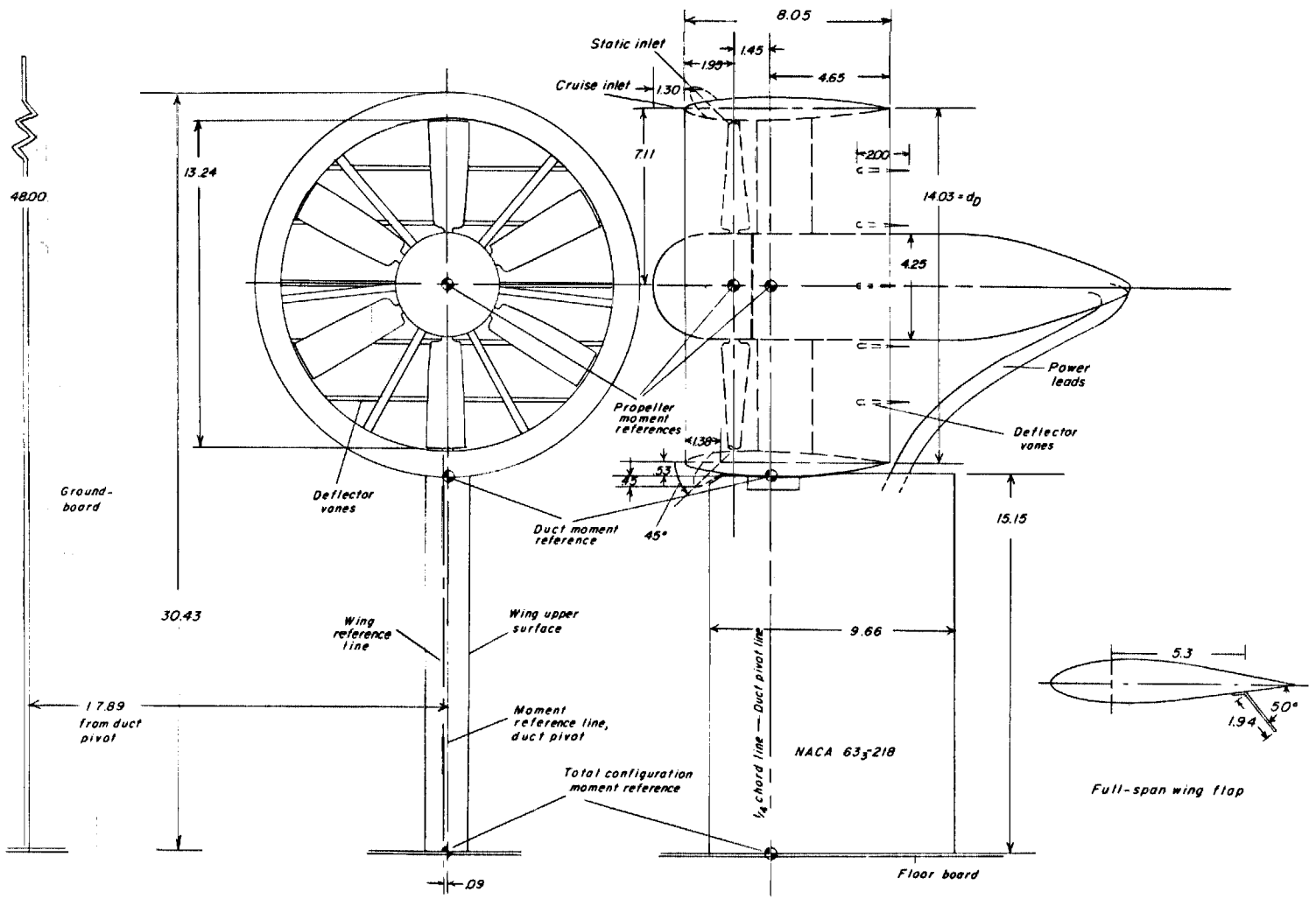

Figure 2.- Drawing of model. All dimensions are in inches.

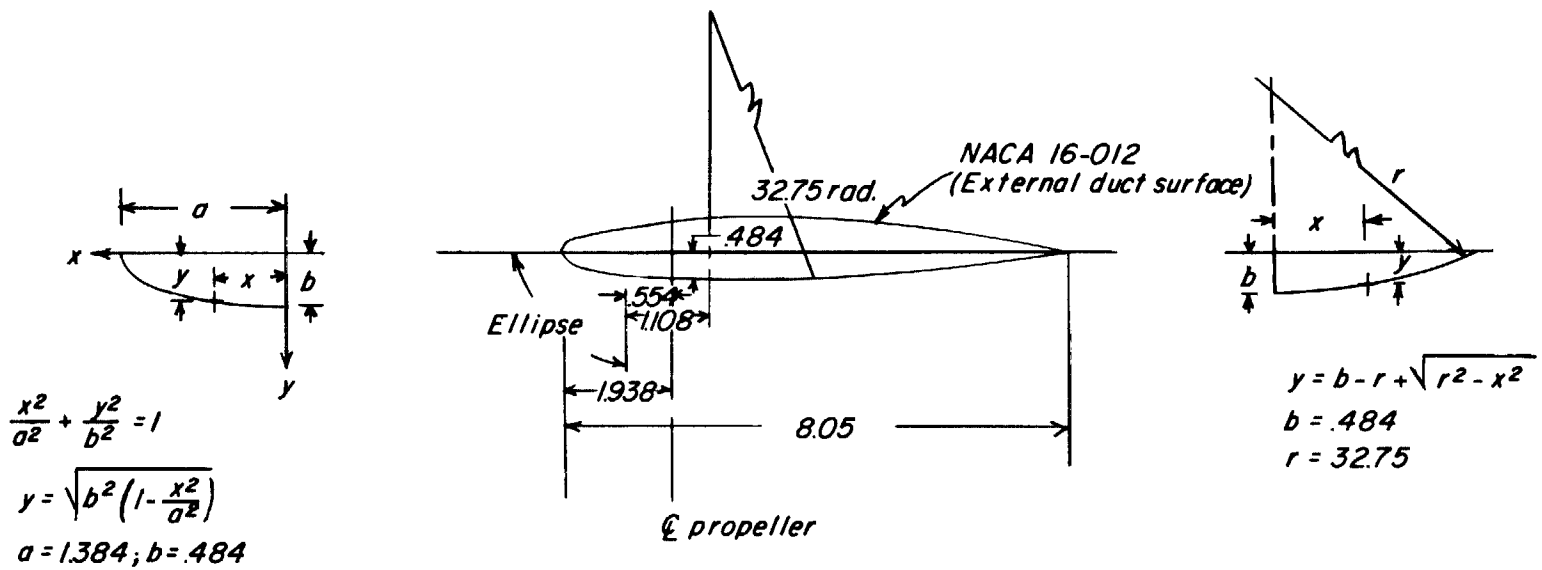

Figure 3.- Duct cross section and definition of duct ordinates. Symbols used to define the duct ordinates are standard mathematical notation and should not be confused with symbols defined elsewhere.

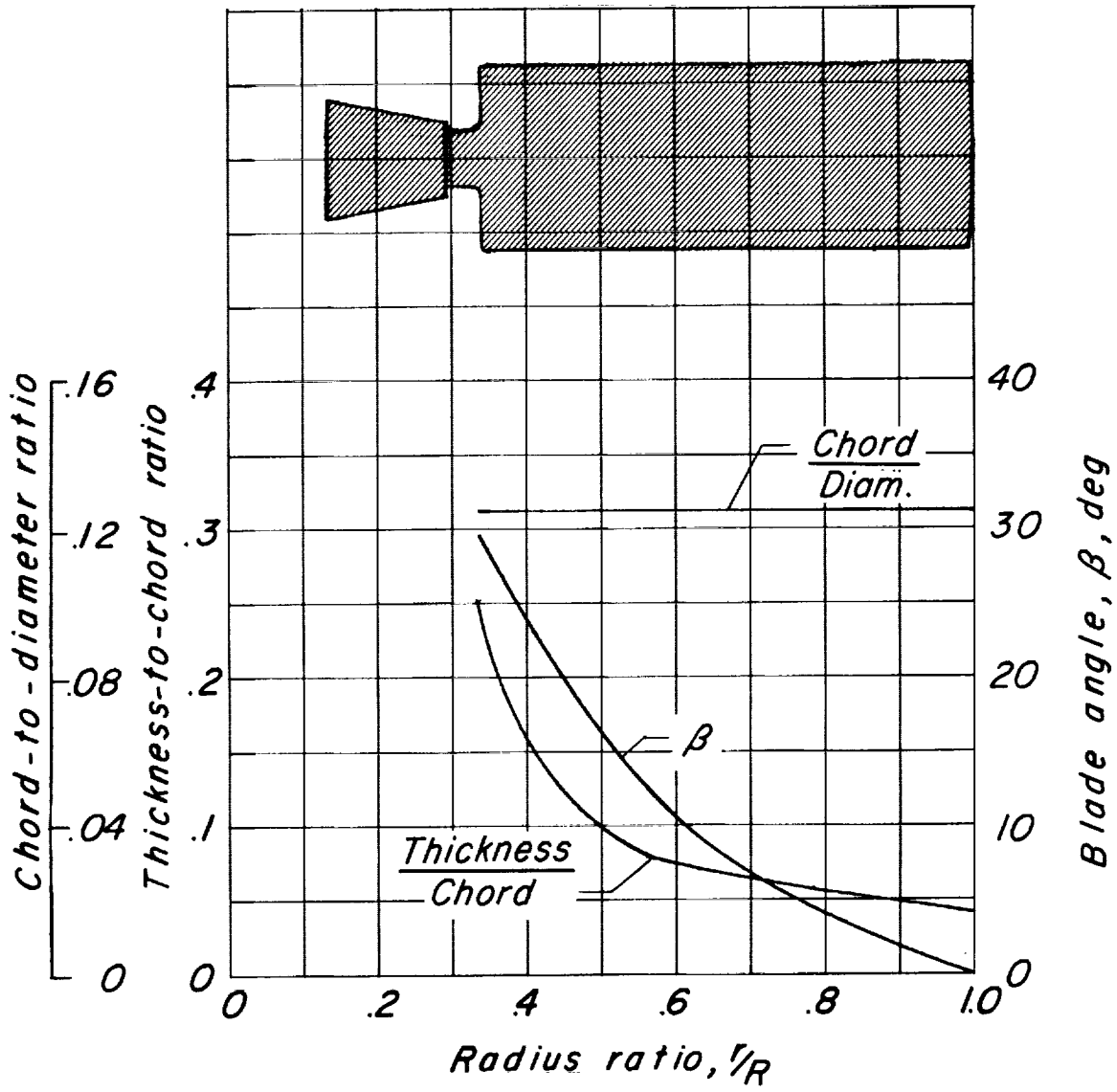

Figure 4.- Propeller-blade geometric characteristics.

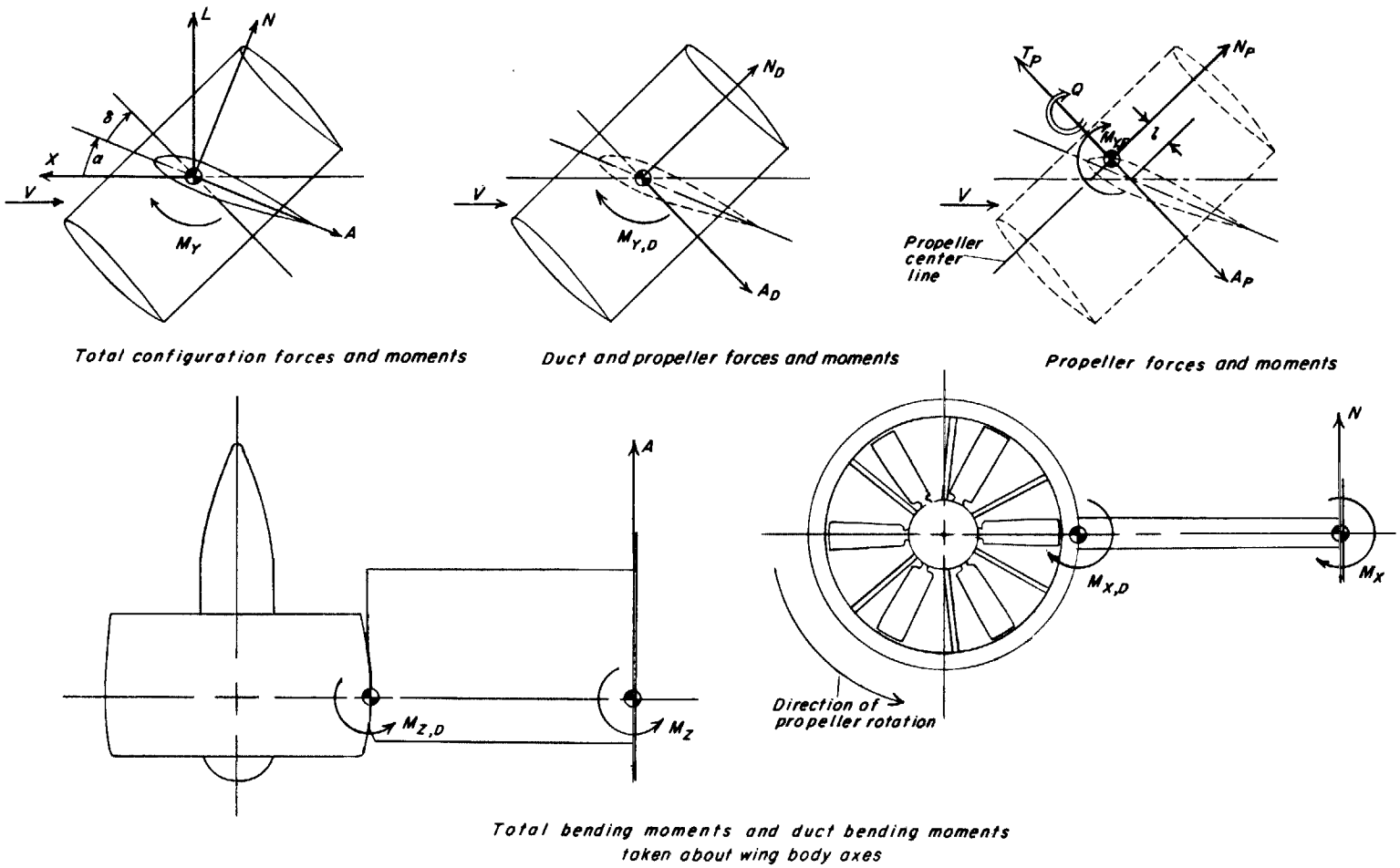

Figure 5.- Positive sense of forces, moments, and angles shown with respect to appropriate reference points.

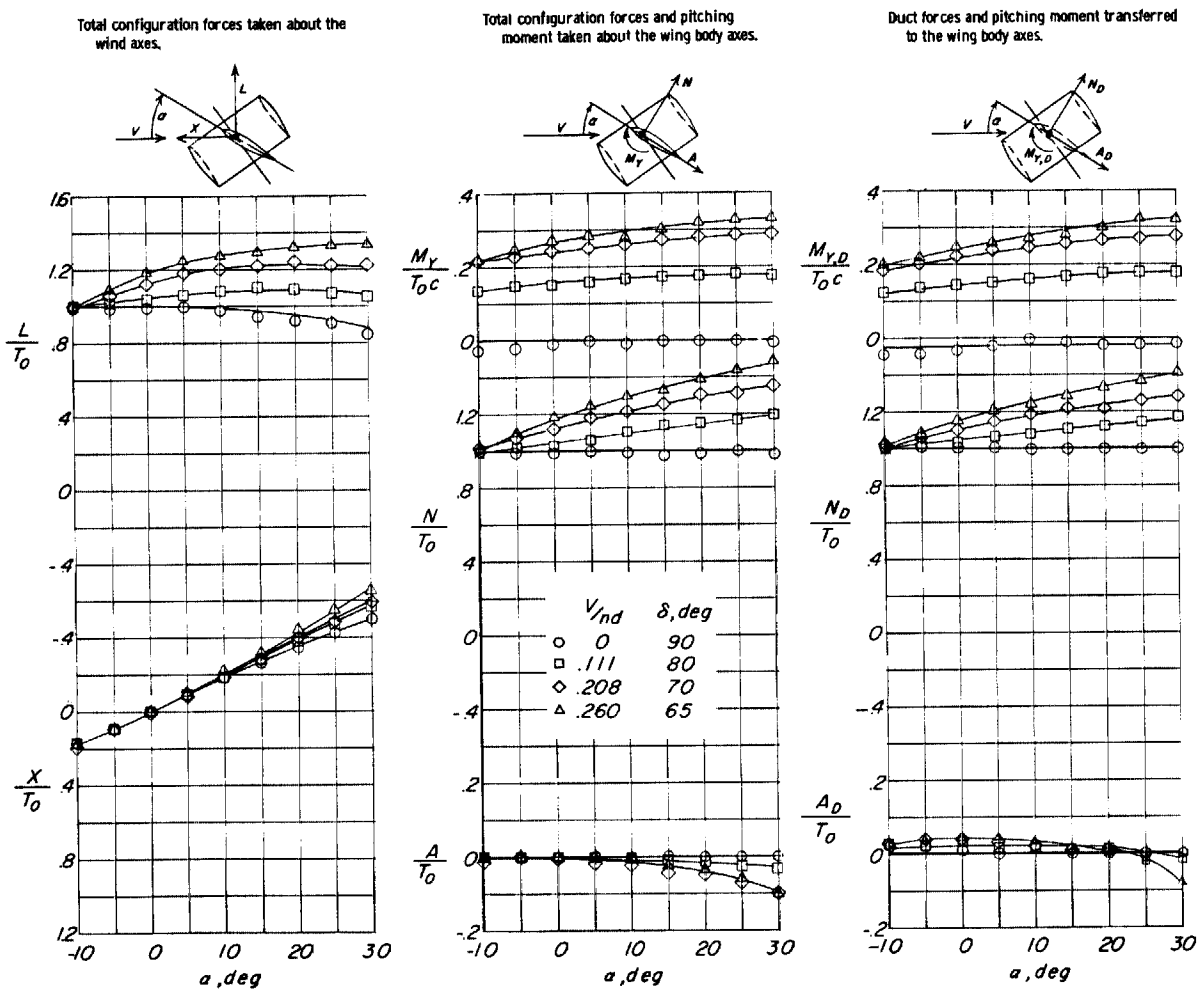

Figure 6.- Aerodynamic characteristics of static duct configuration through a duct-angle and advance-ratio range for a steady level flight condition at $\alpha_{(X=0)} \approx 0^{\circ}$. $h/c = \infty$.

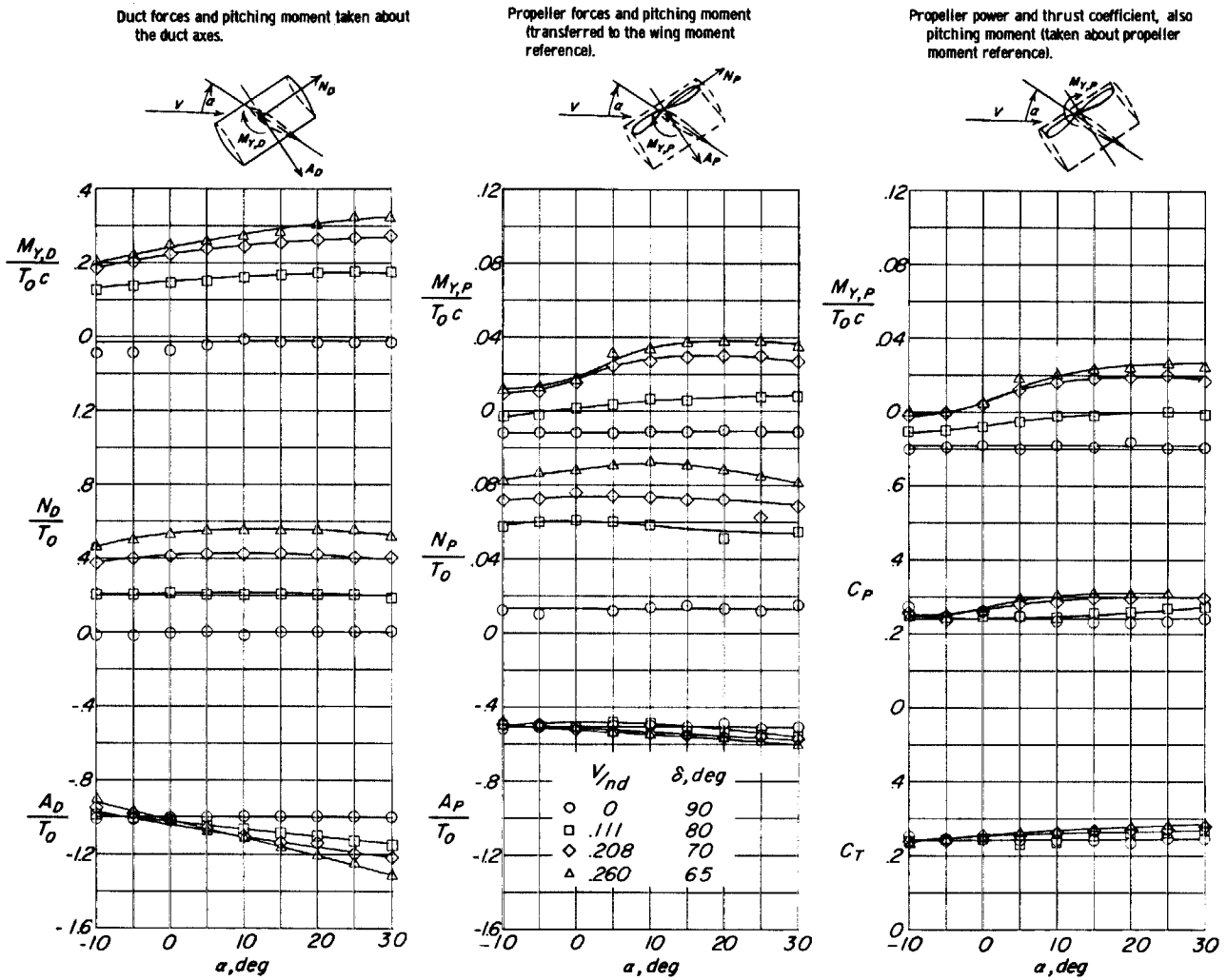

(d) (e) (f)

Figure 6.- Continued.

Bending moments of the total configuration taken about the wing body axes.

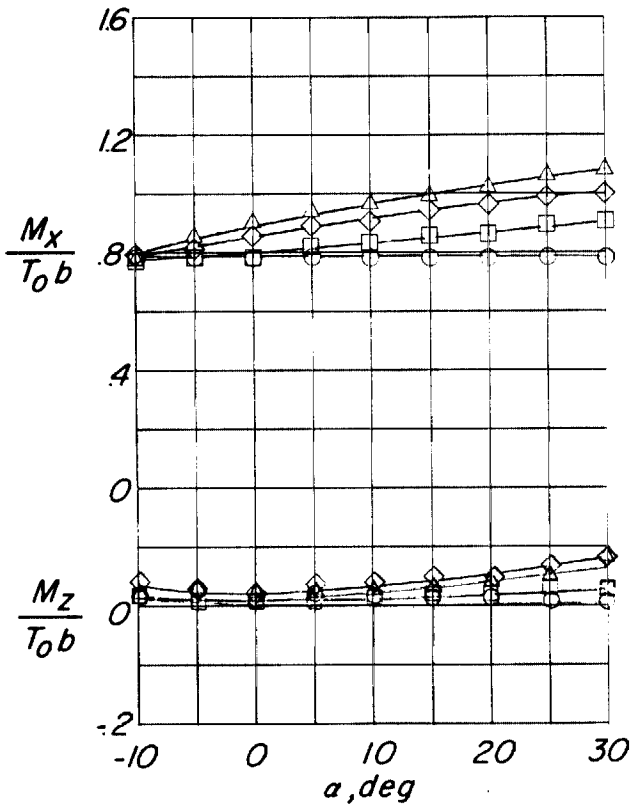

(g)

Bending moment of the duct taken about the wing body axes at the duct moment reference.

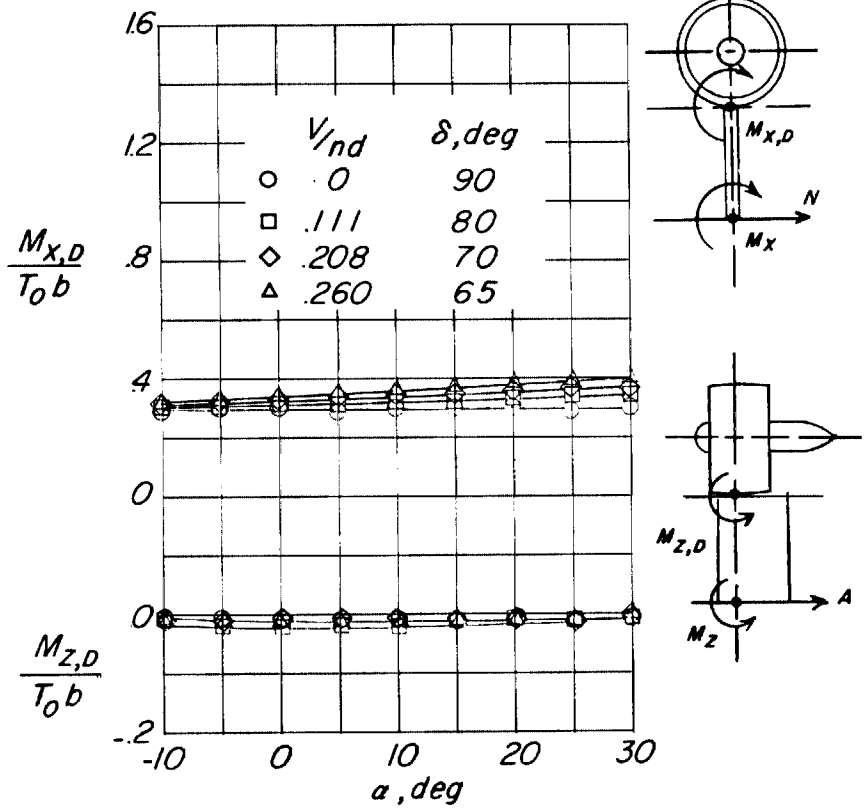

(h)

Figure 6.- Concluded.

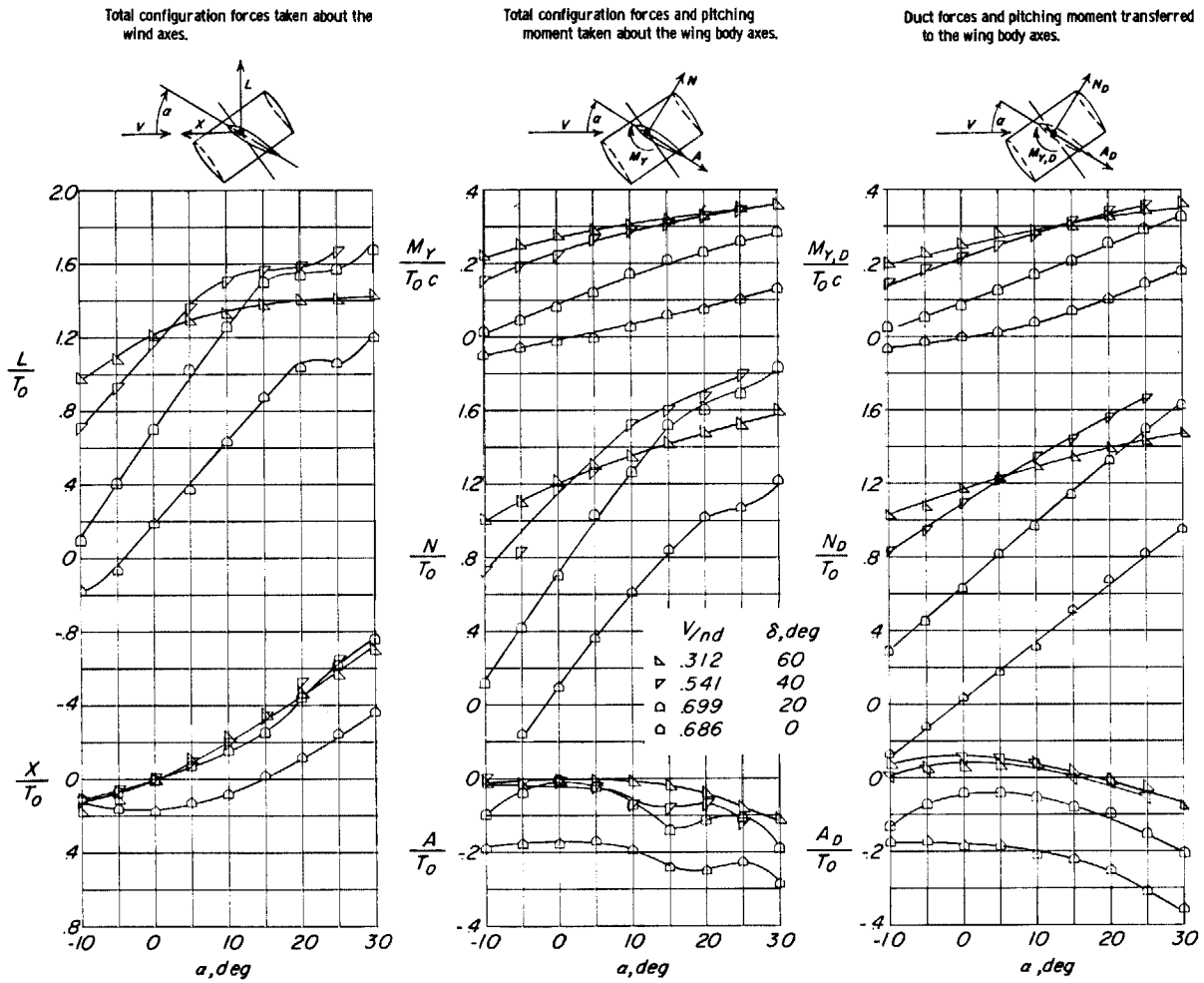

Figure 7.- Aerodynamic characteristics of static duct configuration through a duct-angle and advance-ratio range for a steady level flight condition at $\alpha_{(X=0)} \approx 0^{\circ}$. $h/c = \infty$.

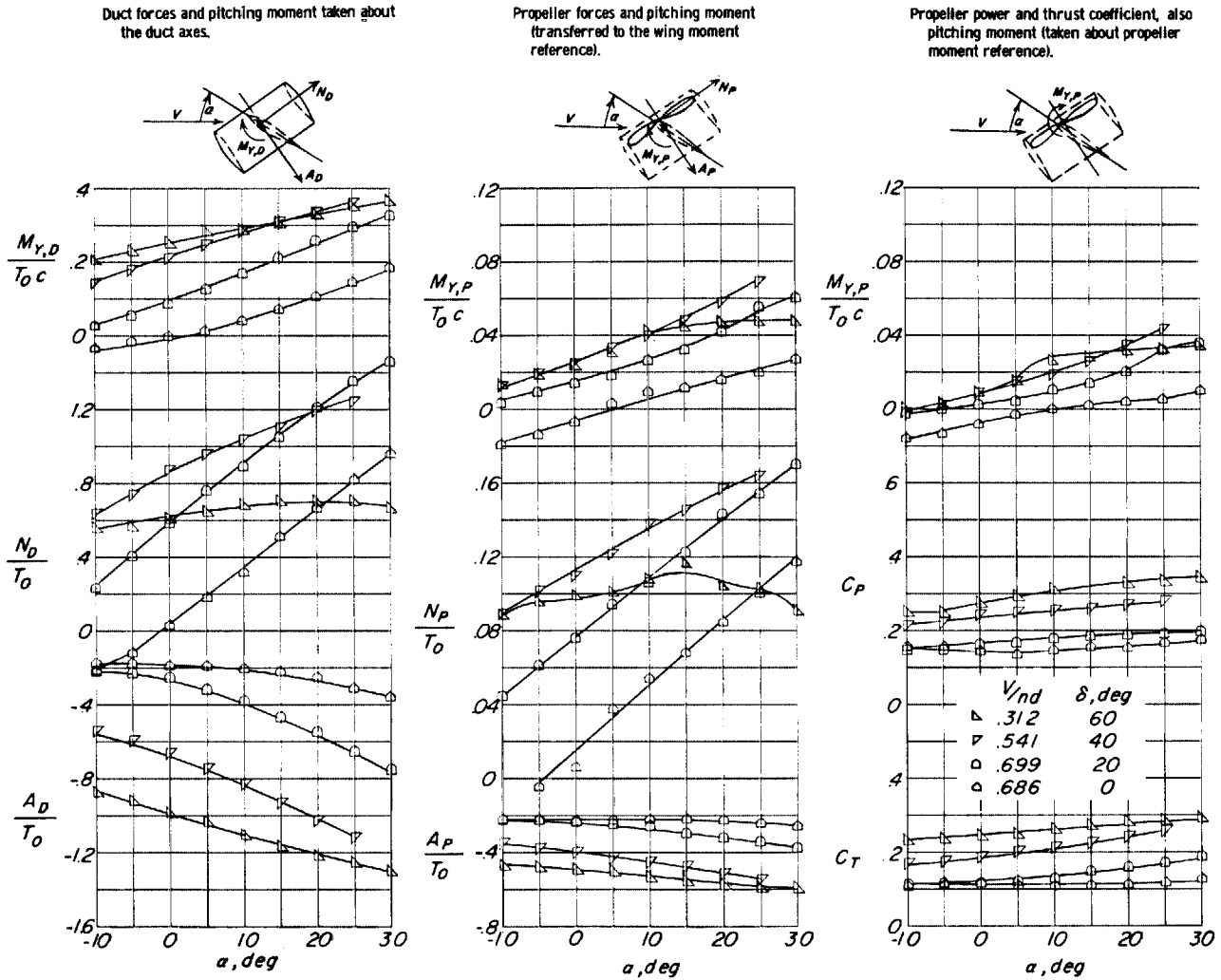

Figure 7.- Continued.

Bending moments of the total configuration taken about the wing body axes.

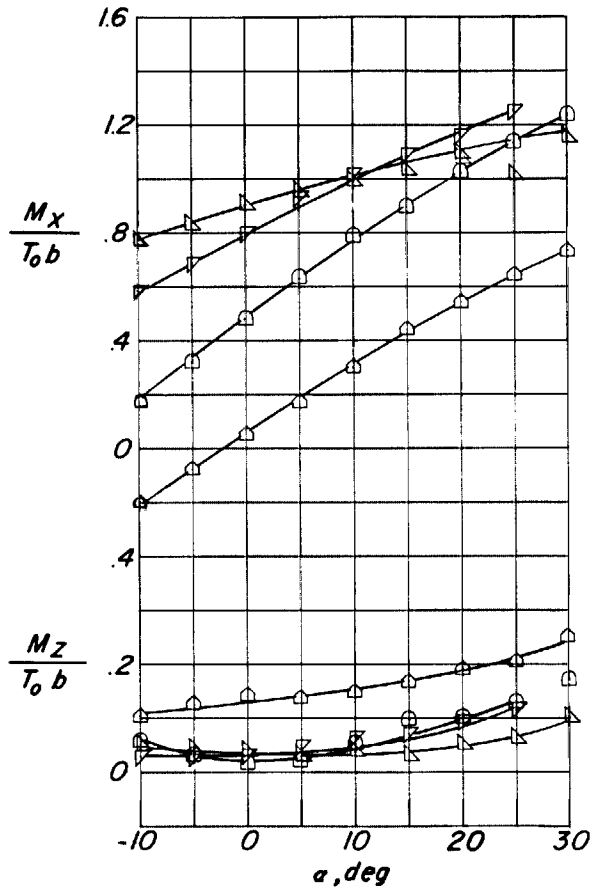

(g)

Bending moment of the duct taken about the wing body axes at the duct moment reference.

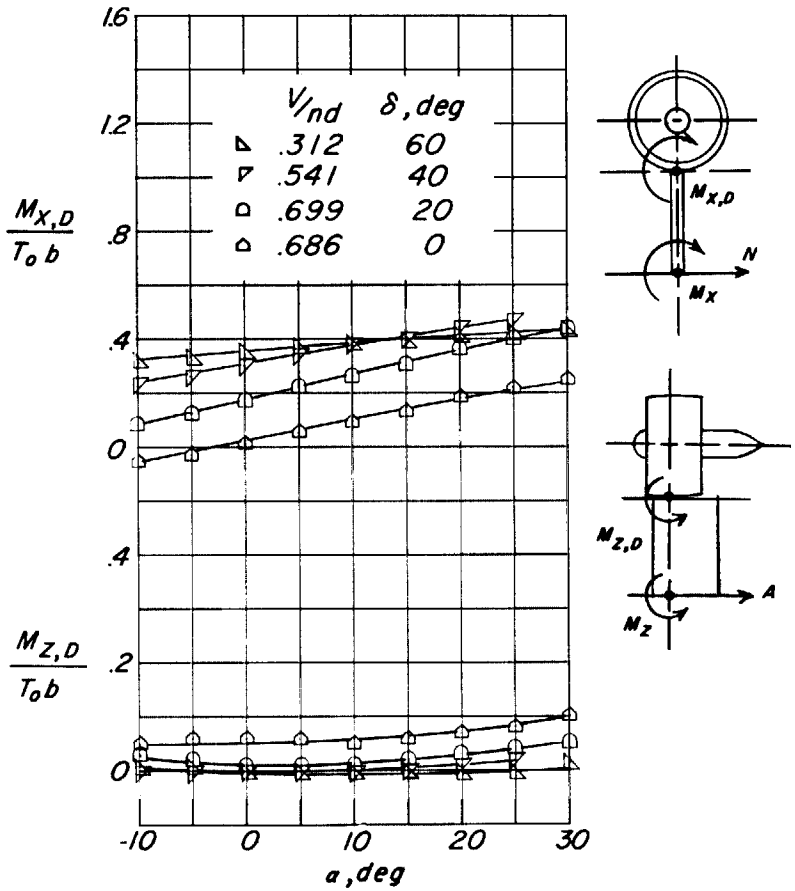

(h)

Figure 7.- Concluded.

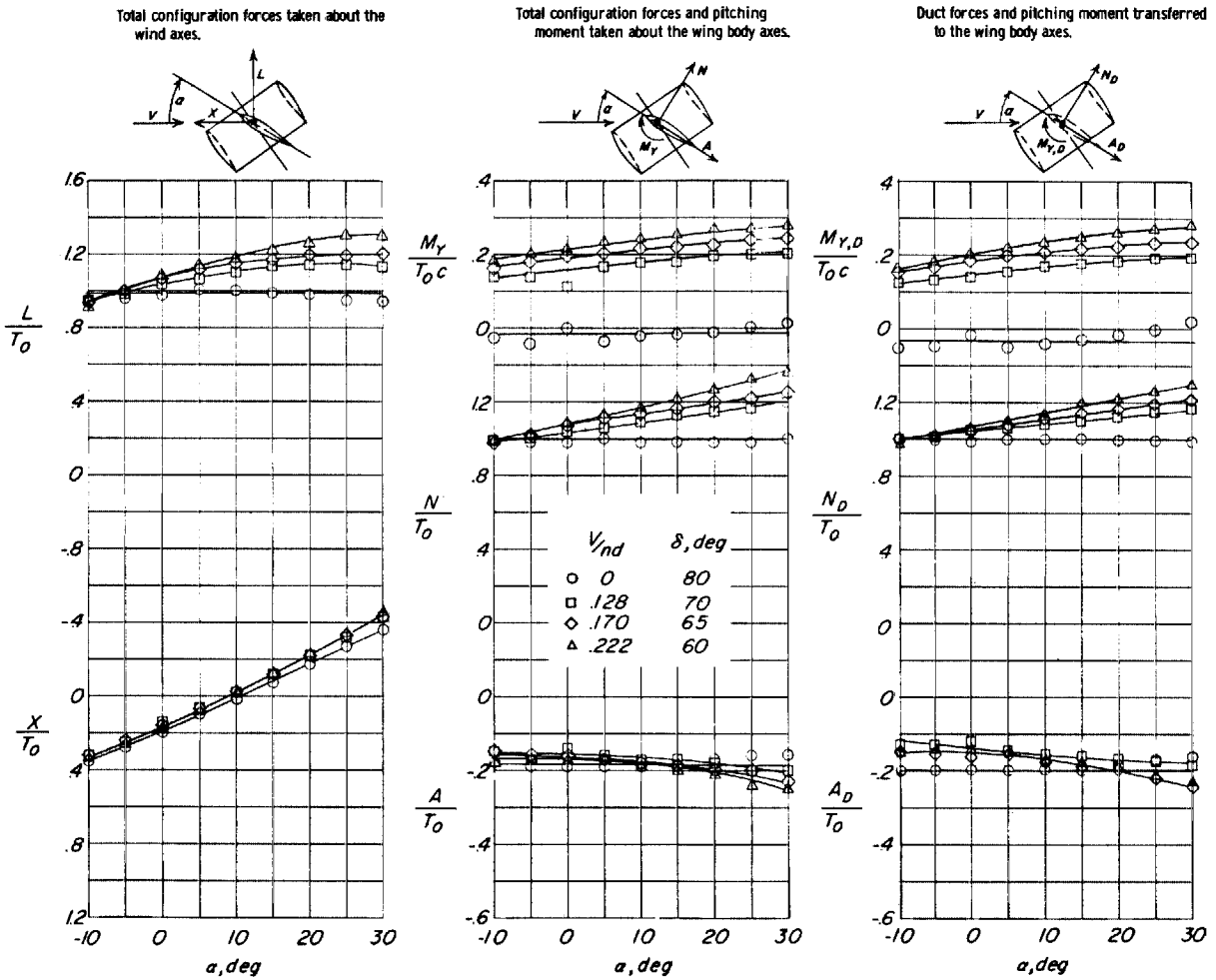

(a) (b) (c)

Figure 8.- Aerodynamic characteristics of static duct configuration through a duct-angle and advance-ratio range for a steady level flight condition at $\alpha_{(X=0)} \approx 10^{\circ}$. $h/c = \infty$.

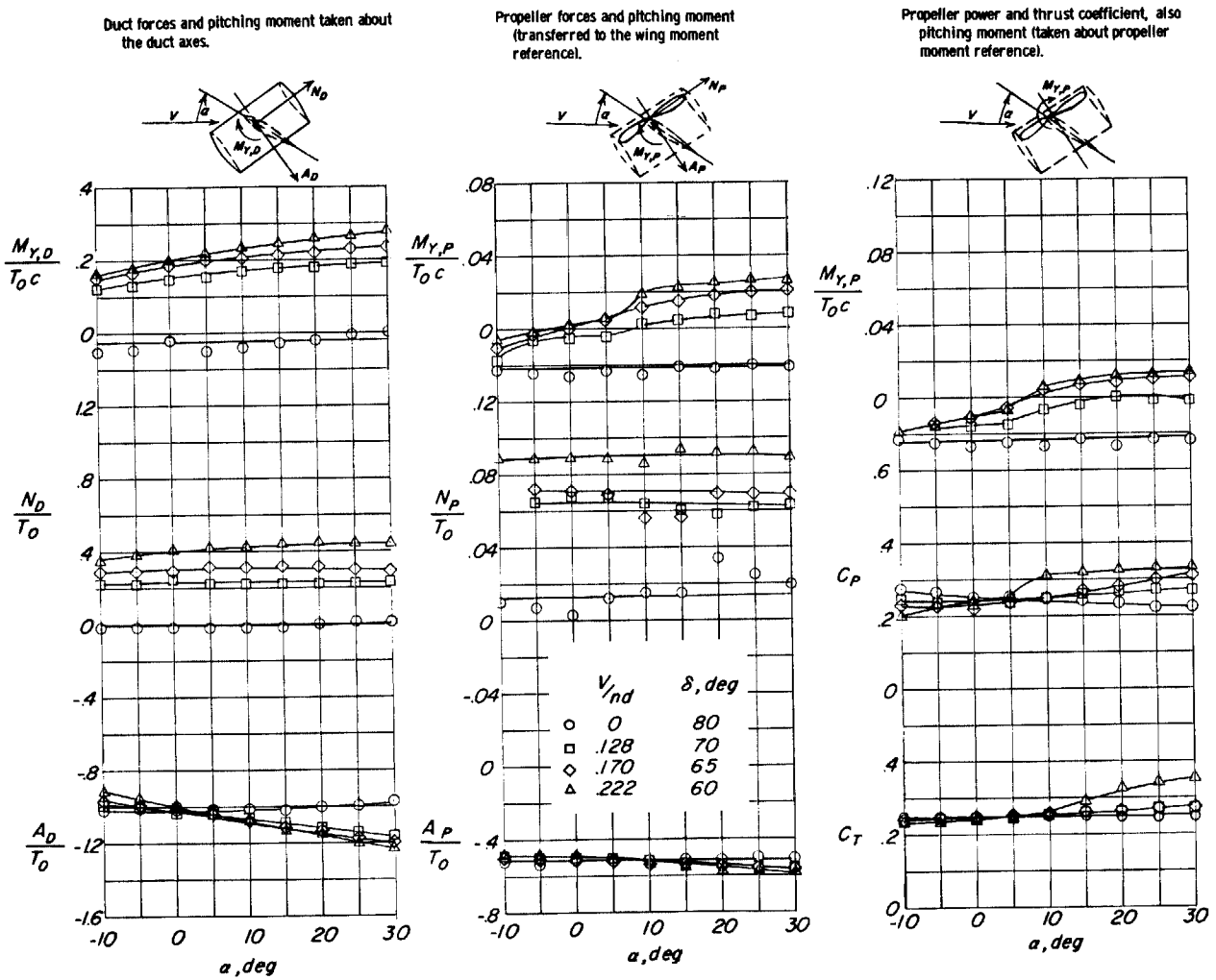

Figure 8.- Continued.

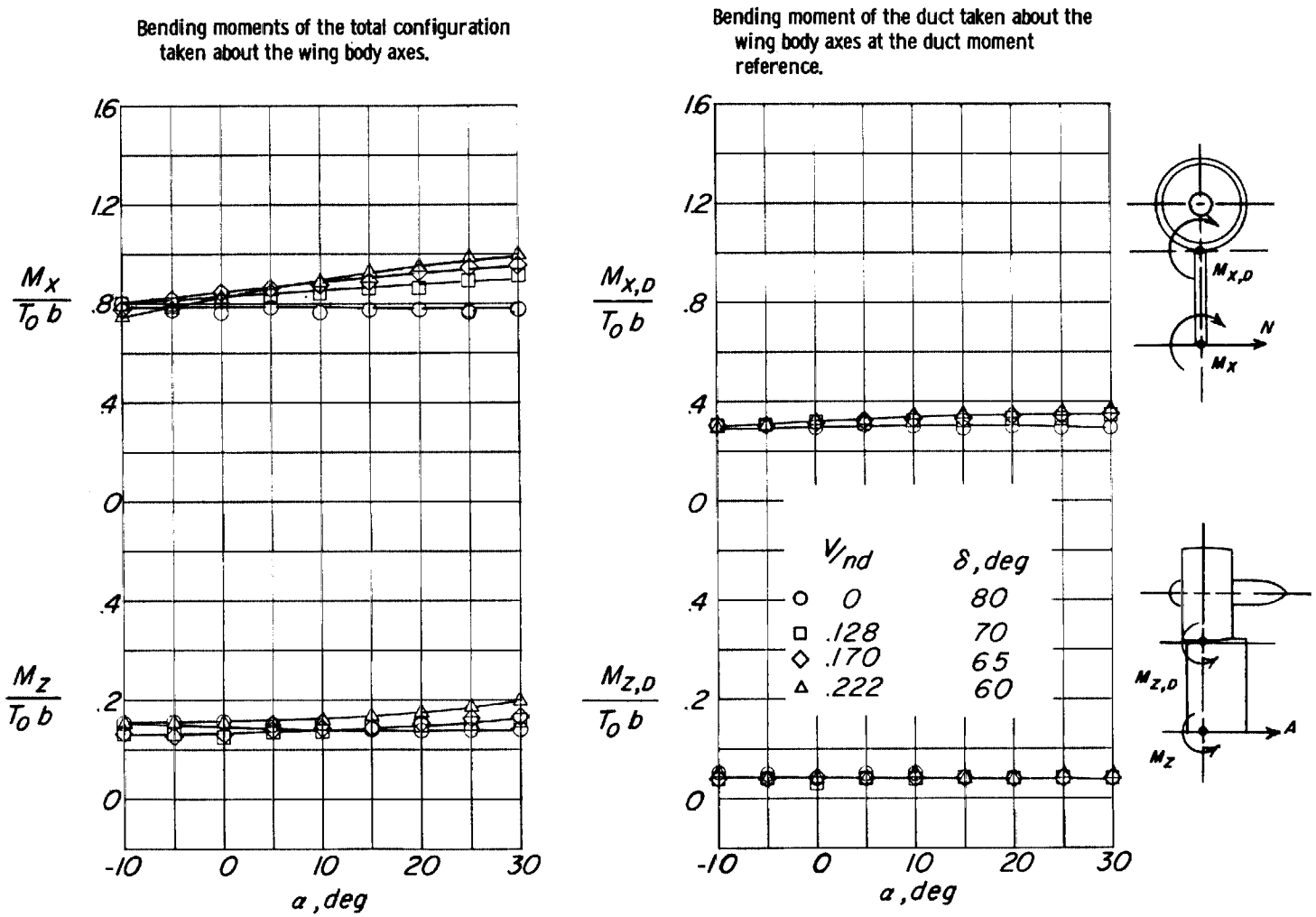

Figure 8.- Concluded.

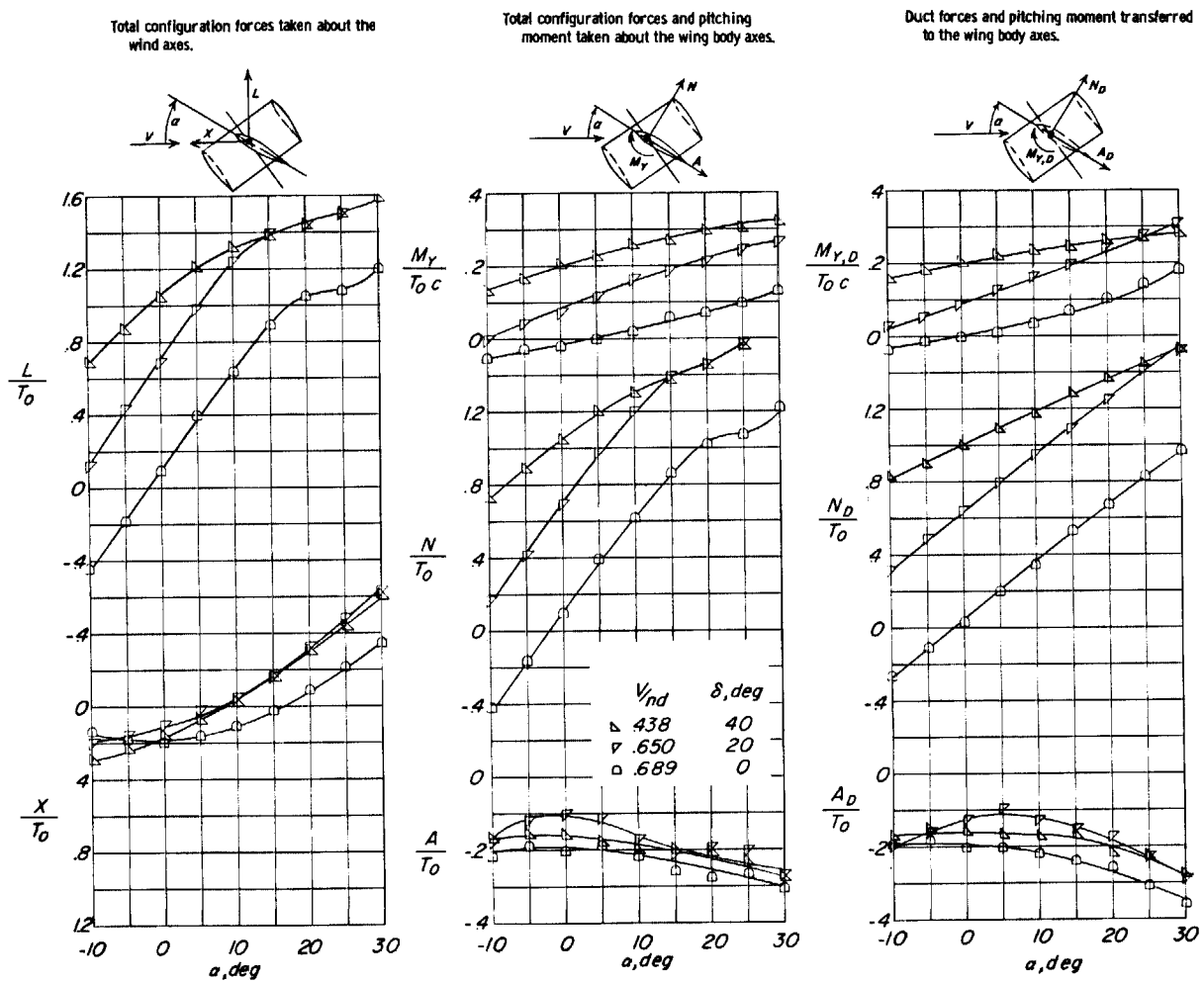

Figure 9.- Aerodynamic characteristics of static duct configuration through a duct-angle and advance-ratio range for a steady level flight condition at $\alpha_{(X=0)} \approx 10^{\circ}$. $h/c = \infty$.

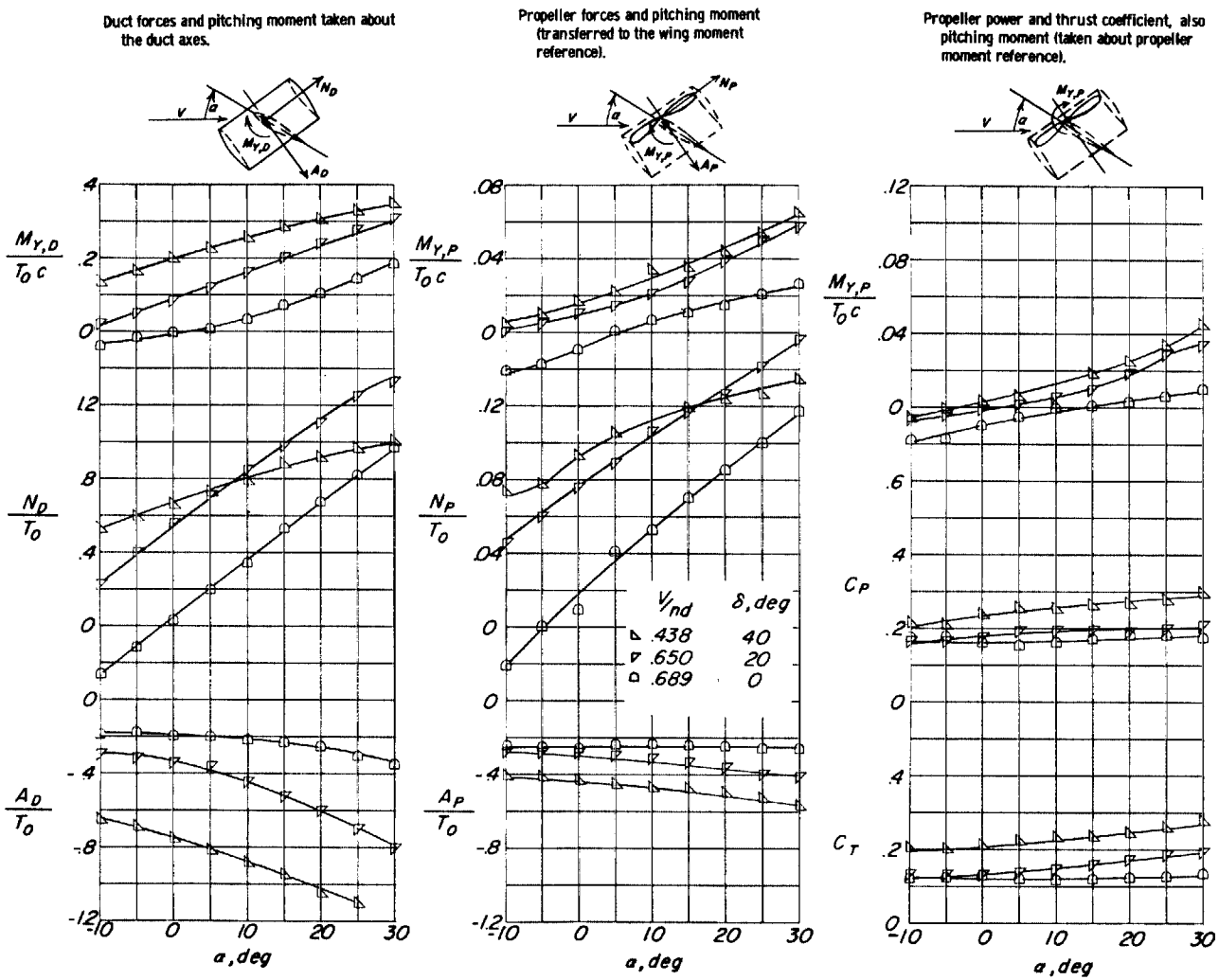

Figure 9.- Continued.

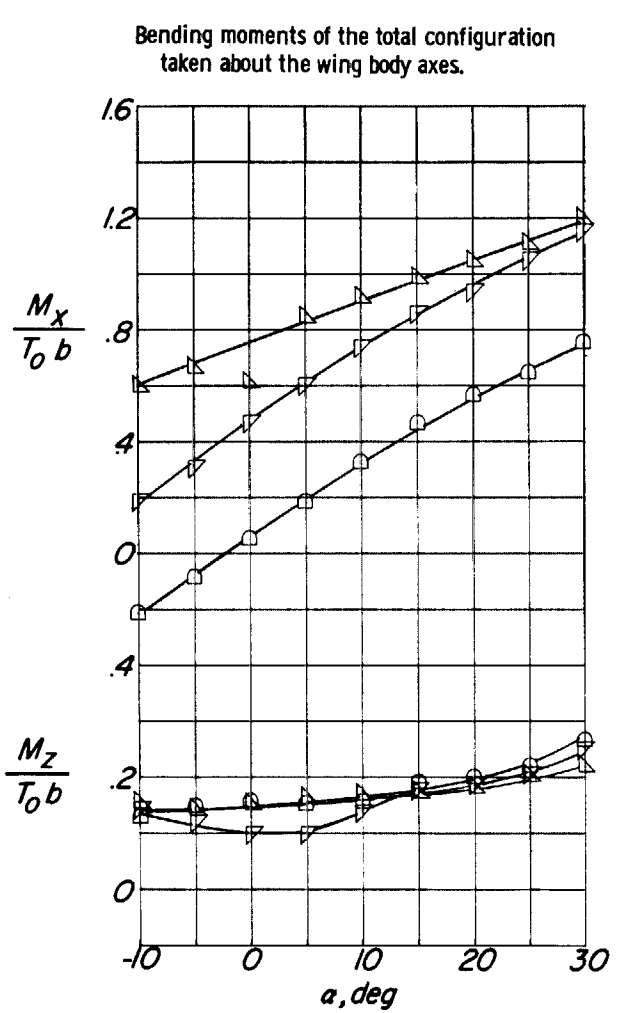

(g)

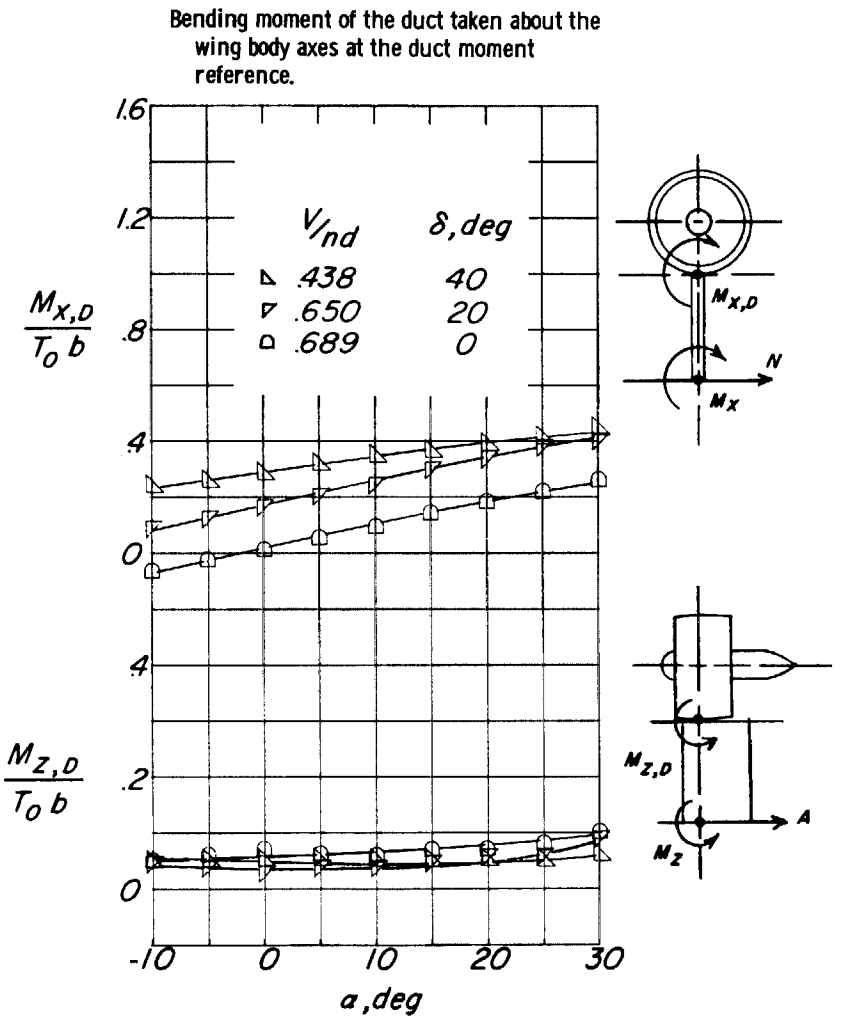

(h)

Figure 9.- Concluded.

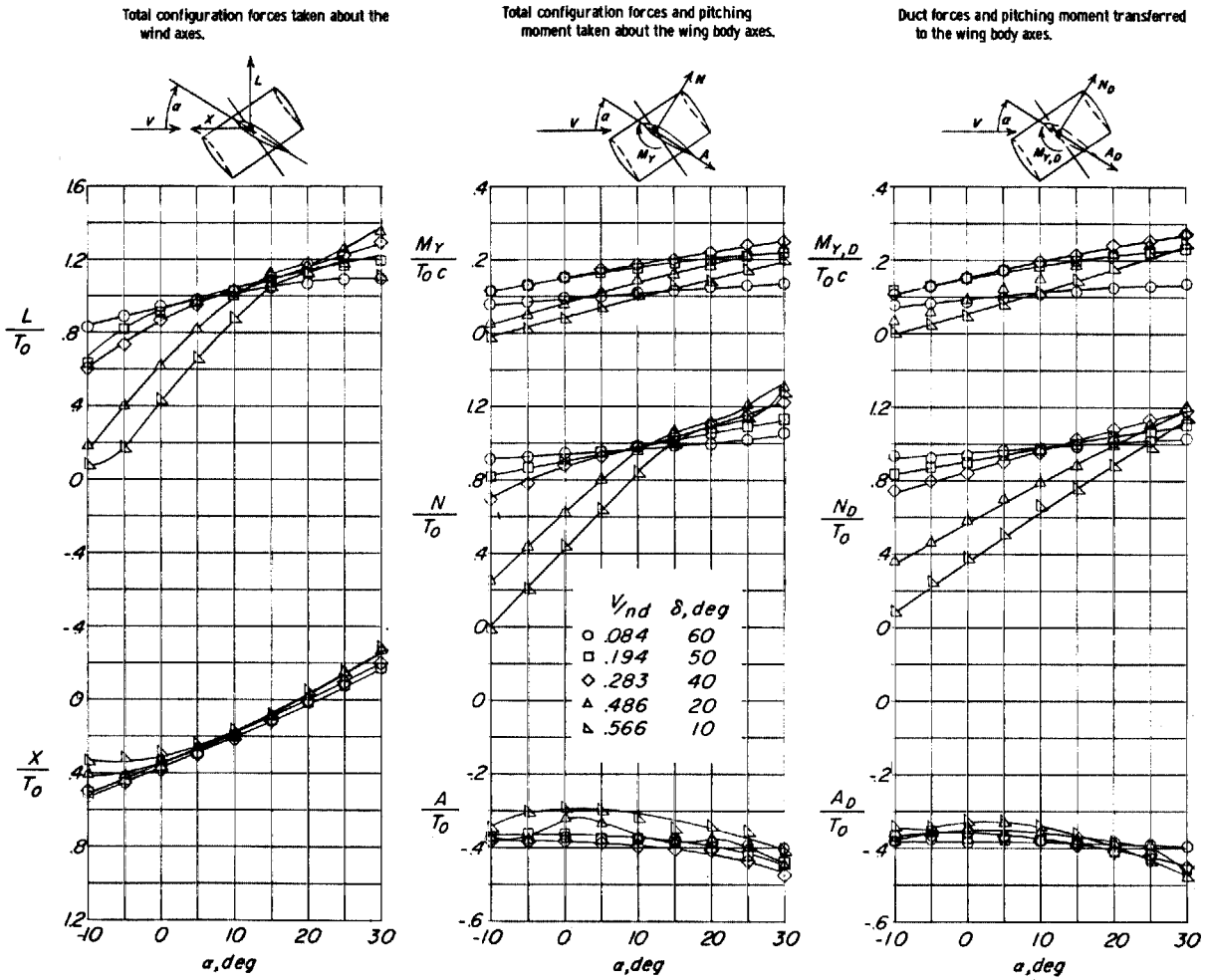

Figure 10.- Aerodynamic characteristics of static duct configuration through a duct-angle and advance-ratio range for an accelerating flight condition at $\alpha \approx 10^{\circ}$. $h/c = \infty$.

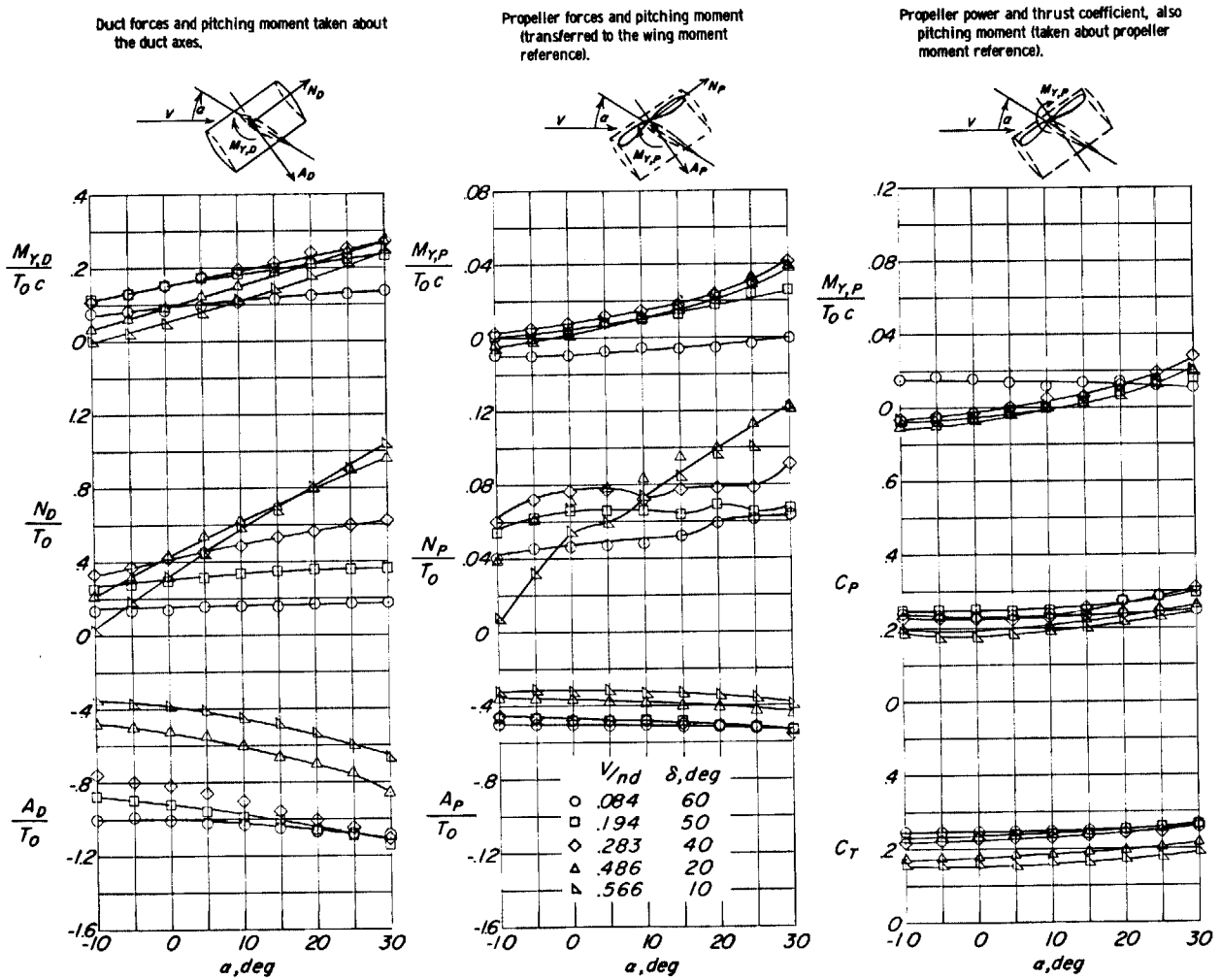

Figure 10.- Continued.

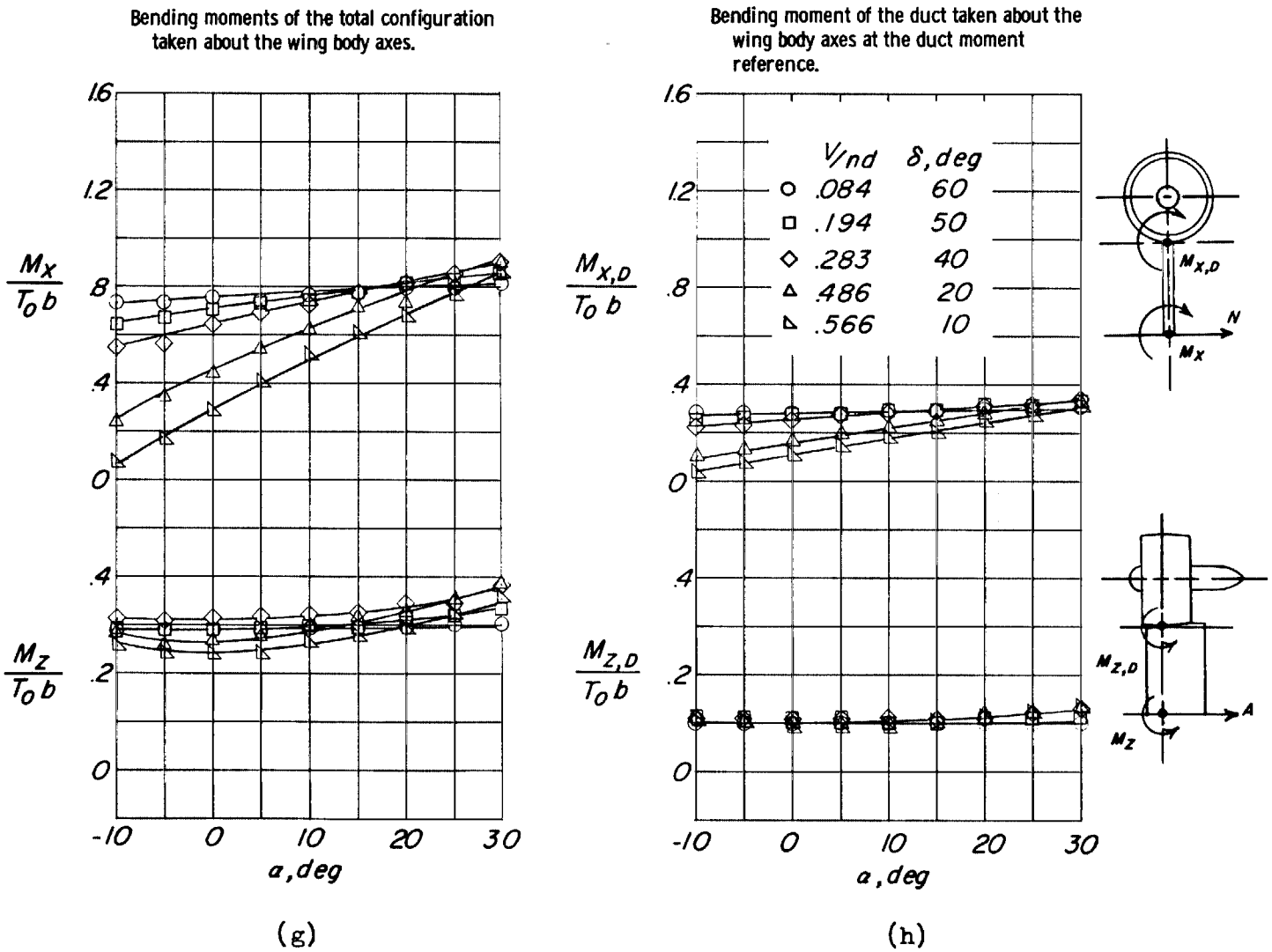

Figure 10.- Concluded.

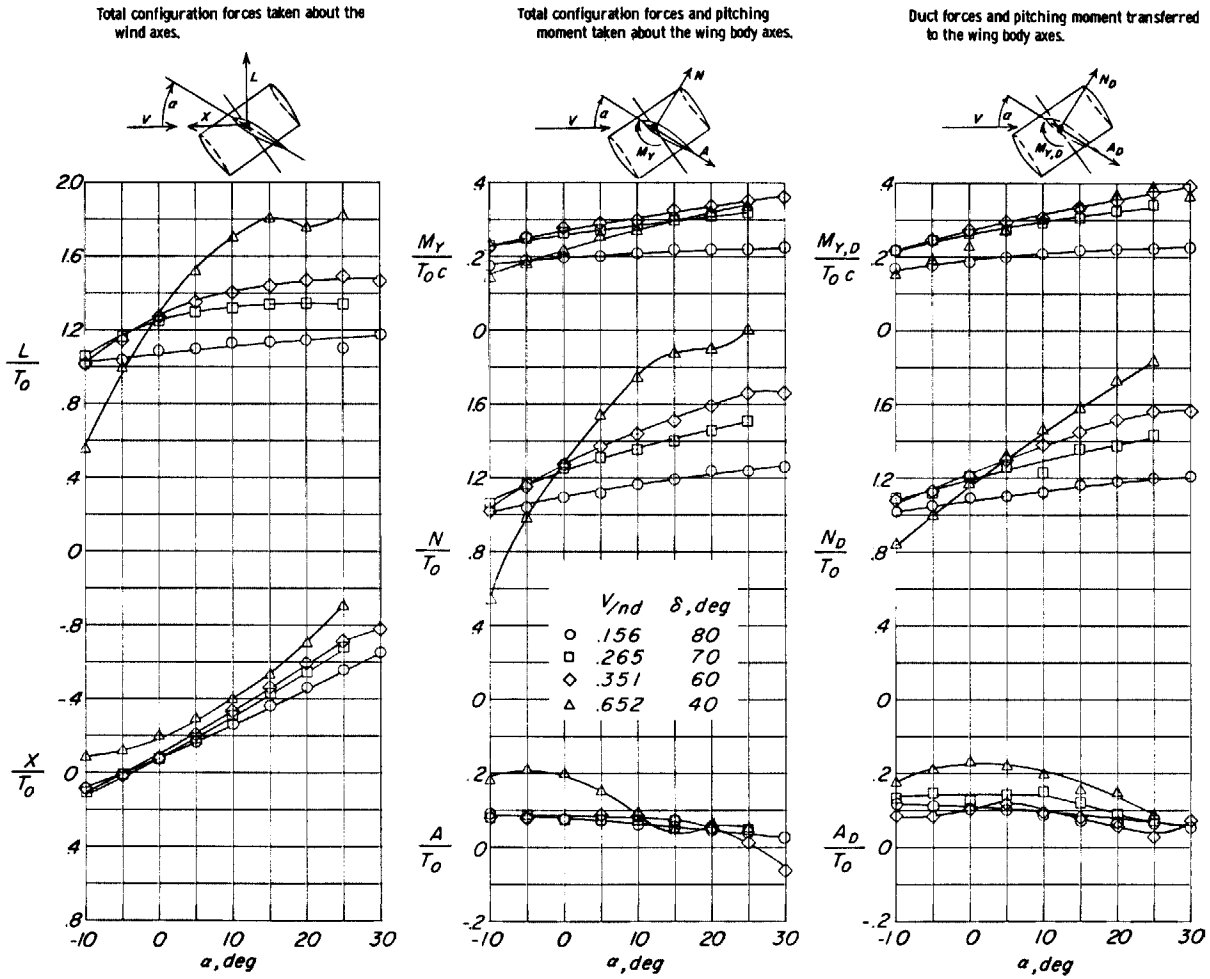

Figure 11.- Aerodynamic characteristics of static duct configuration through a duct-angle and advance-ratio range for a decelerating flight condition at $\alpha \approx 10^{\circ}$. $h/c = \infty$.

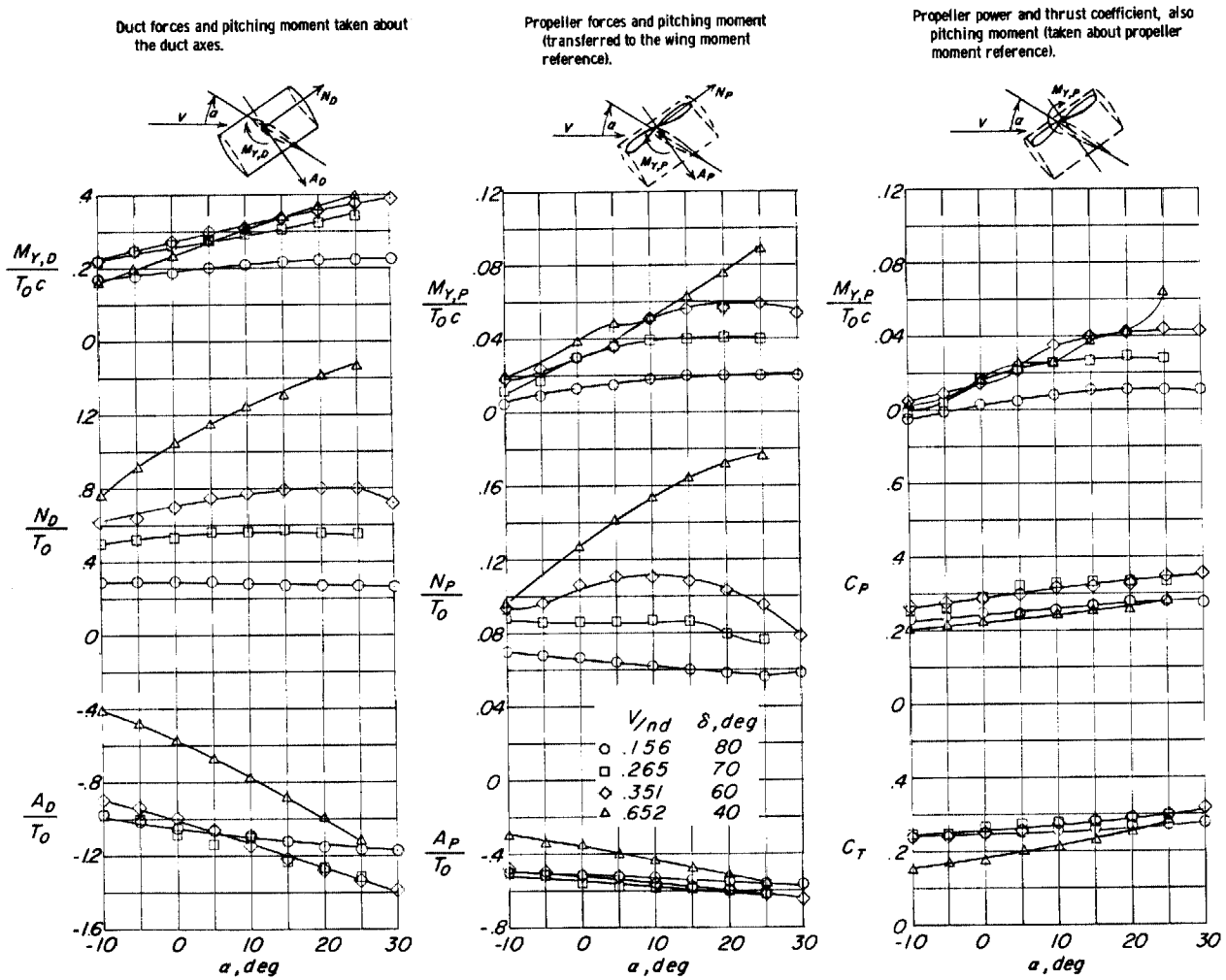

Figure 11.- Continued.

Bending moments of the total configuration taken about the wing body axes.

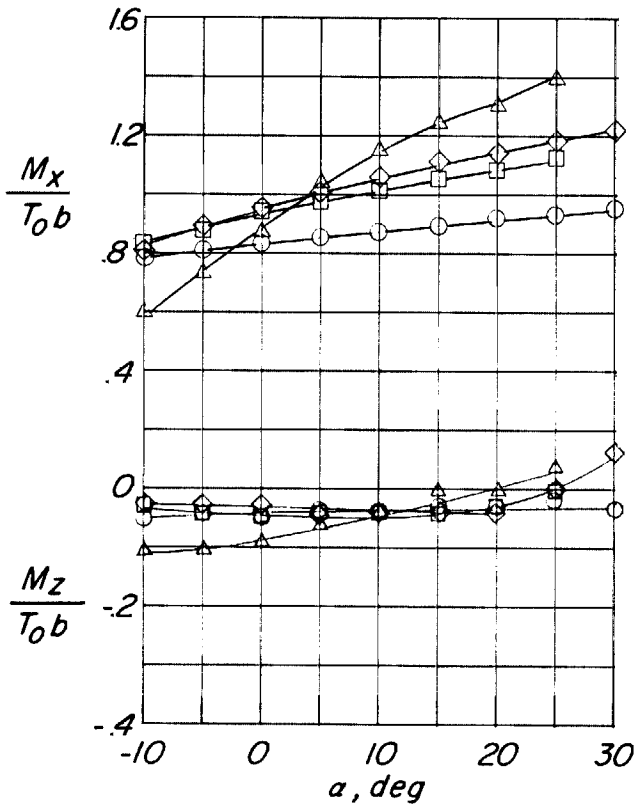

(g)

Bending moment of the duct taken about the wing body axes at the duct moment reference.

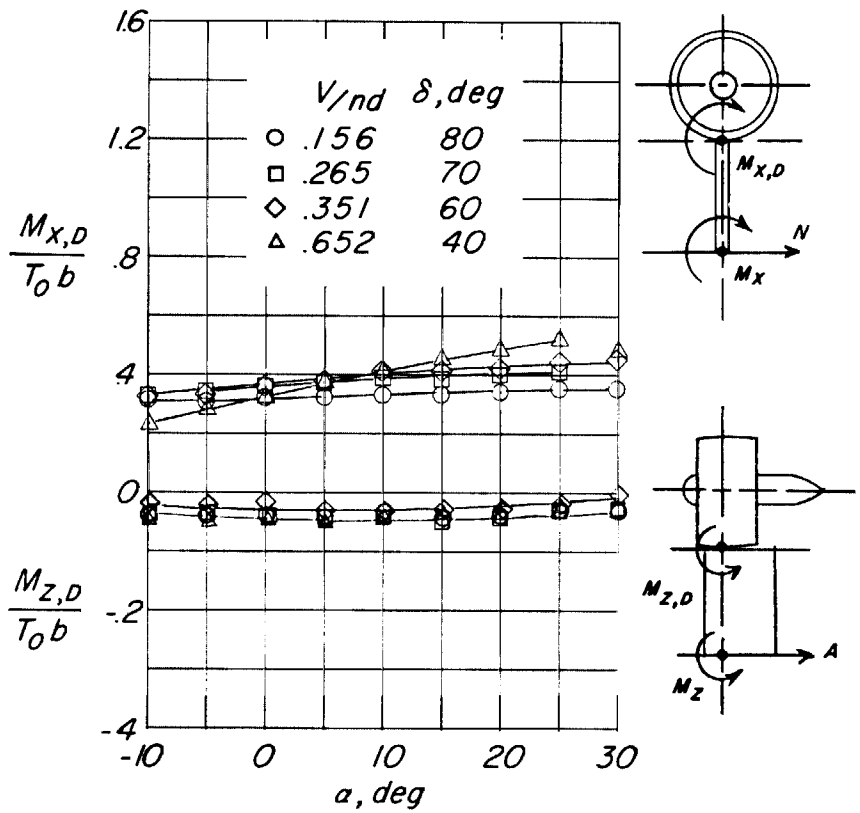

(h)

Figure 11.- Concluded.

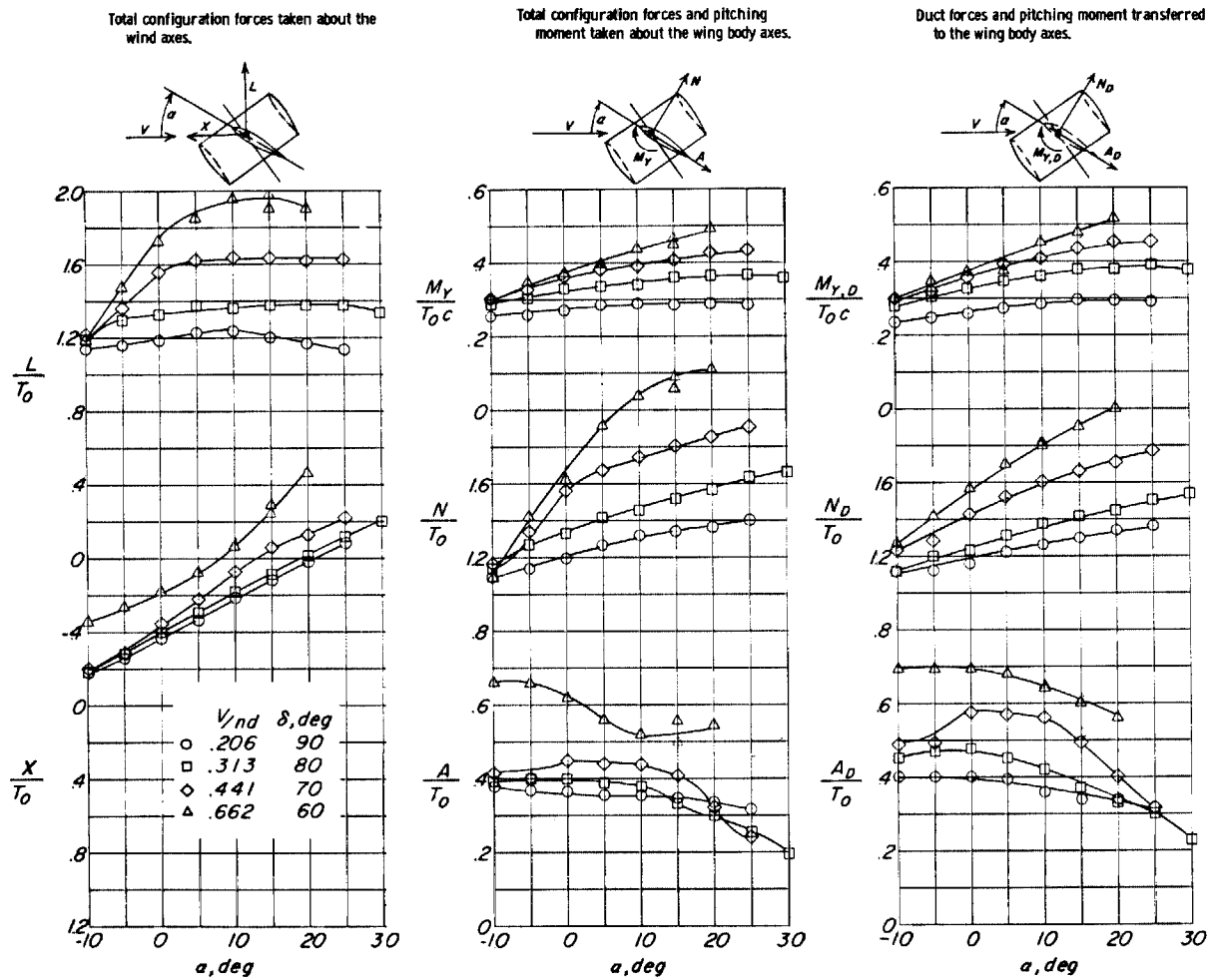

Figure 12.- Aerodynamic characteristics of static duct configuration through a duct-angle and advance-ratio range for a decelerating flight condition at $\alpha \approx 10^{\circ}$. $h/c = \infty$.

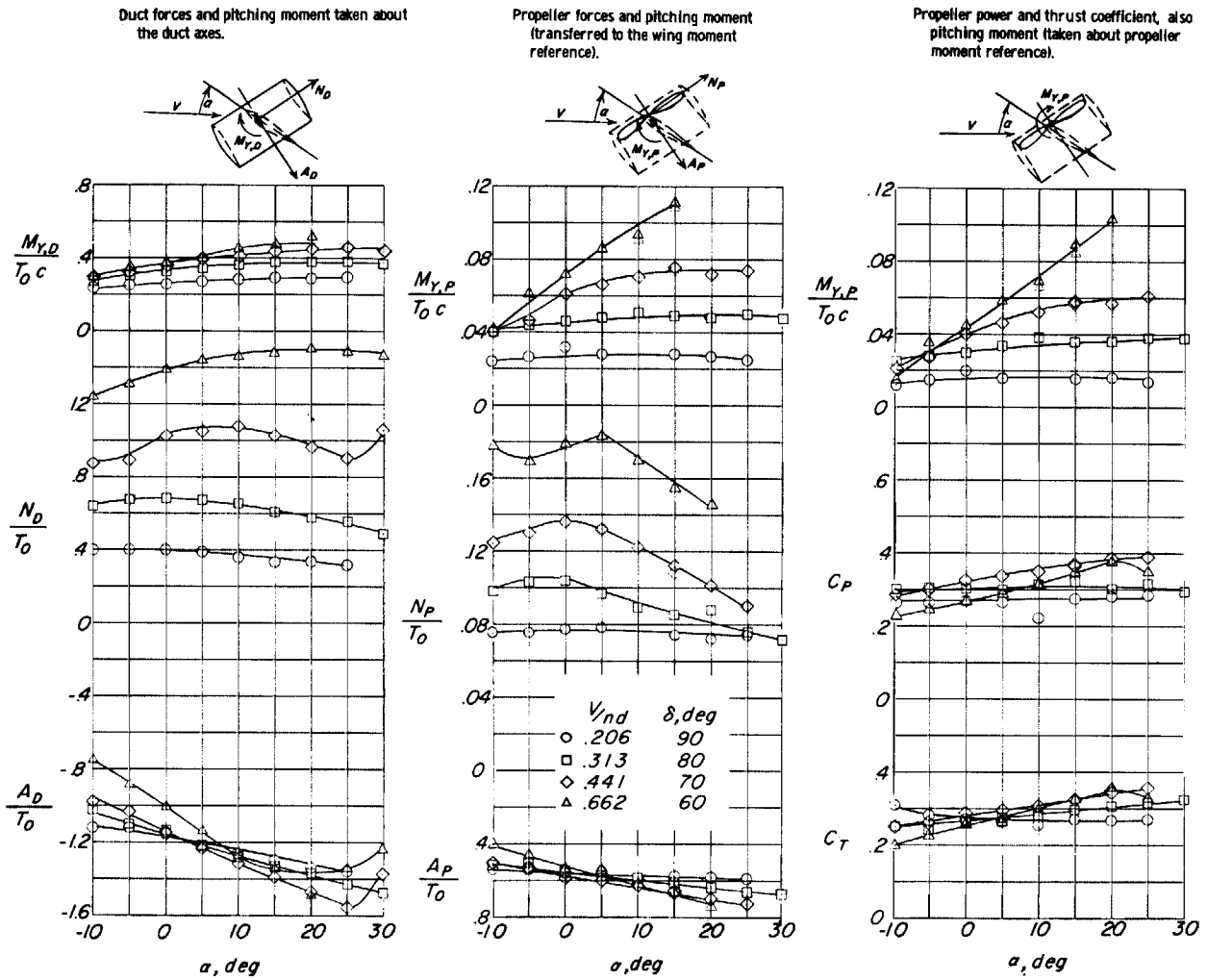

(d) (e) (f)

Figure 12.- Continued.

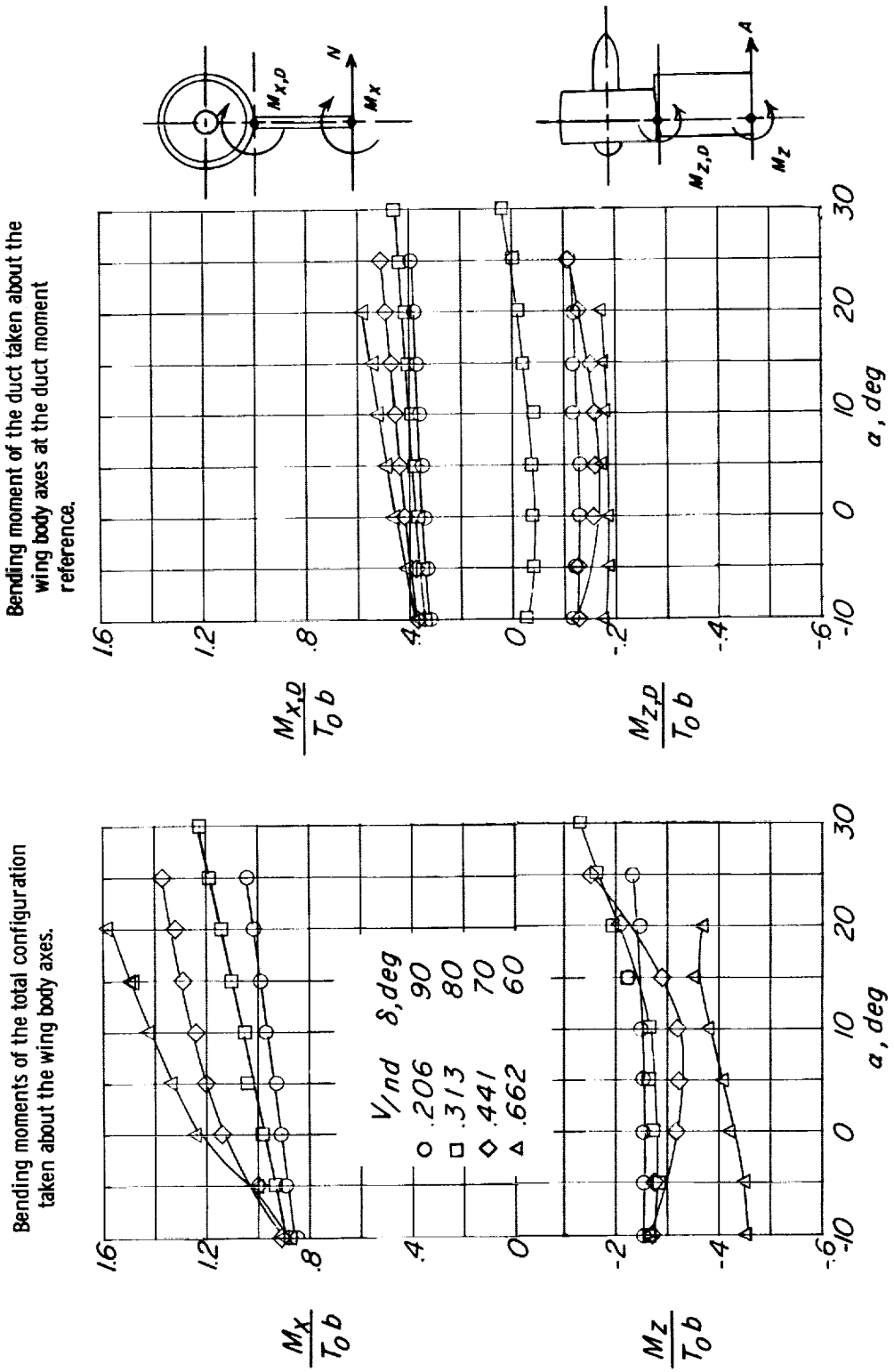

Figure 12.- Concluded.

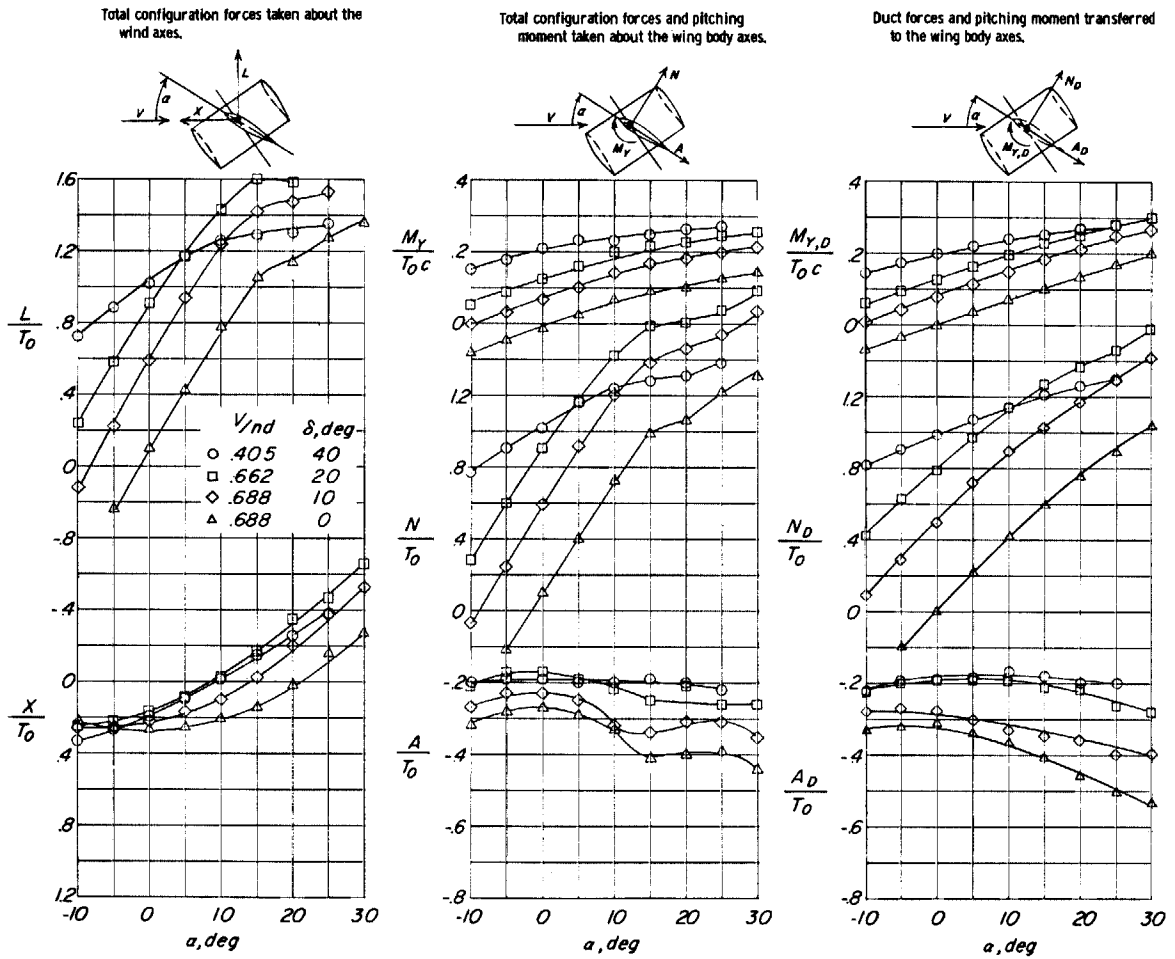

Figure 13.- Aerodynamic characteristics of cruise duct configuration through a low duct-angle range and an advance-ratio range for a steady level flight condition at $\alpha_{(X=0)} \approx 10^{\circ}$. $h/c = \infty$.

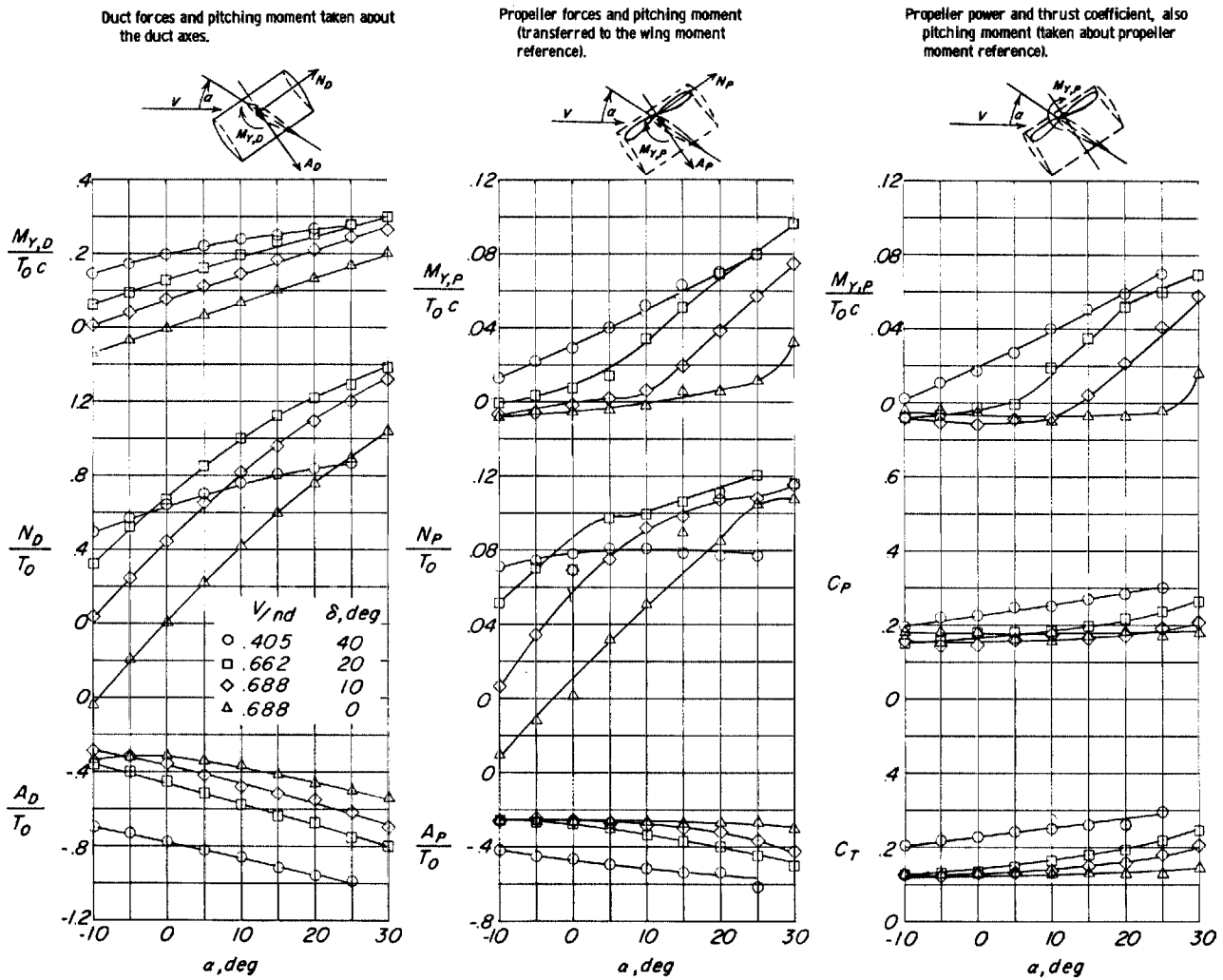

Figure 13.- Continued.

Bending moments of the total configuration taken about the wing body axes.

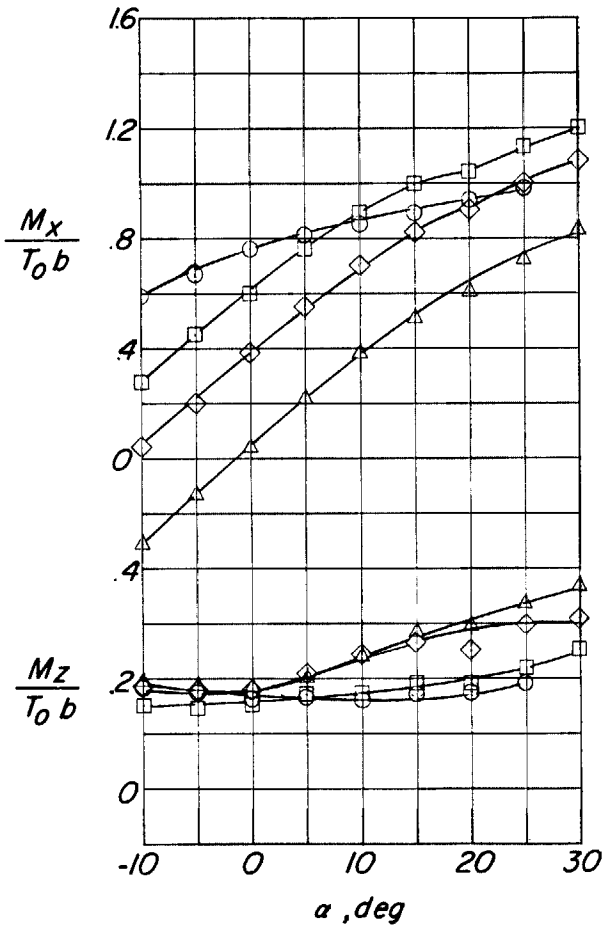

(g)

Bending moment of the duct taken about the wing body axes at the duct moment reference.

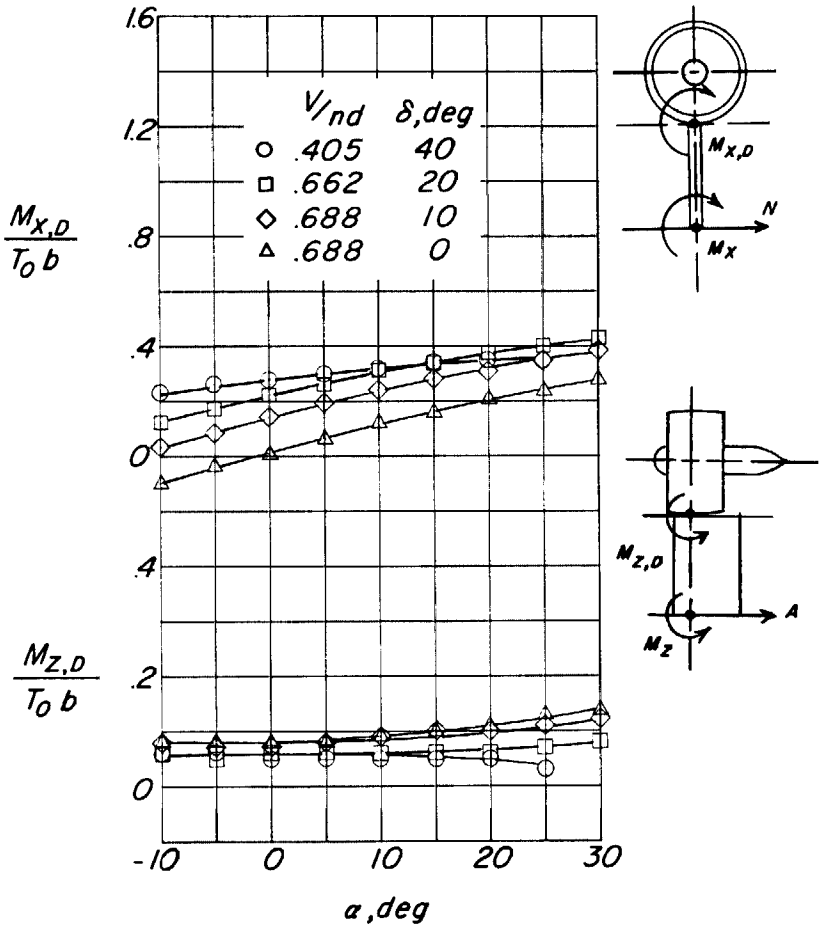

(h)

Figure 13.- Concluded.

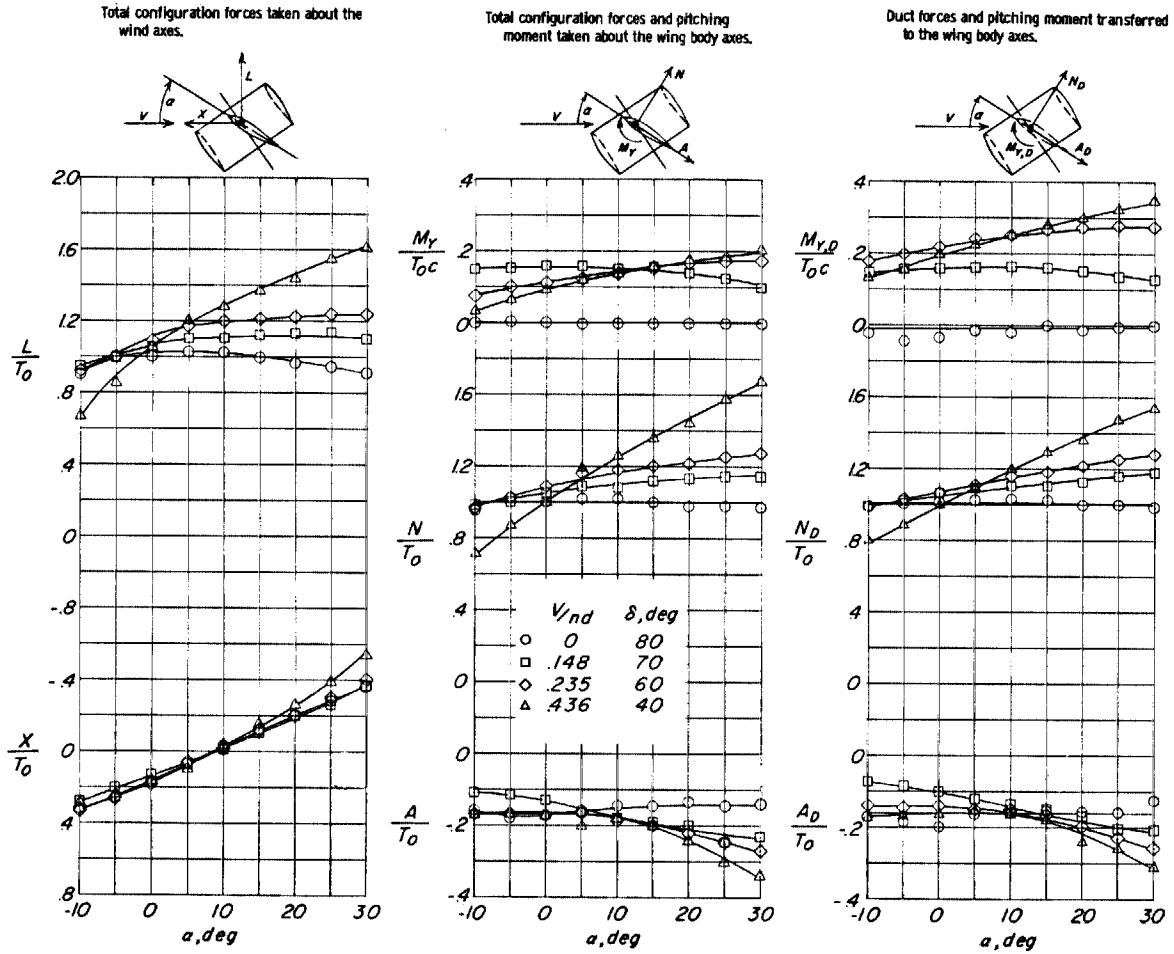

(a) (b) (c)

Figure 14.- Aerodynamic characteristics of static duct configuration through a duct-angle and advance-ratio range, in ground effect (h/c = 1.85), for a steady level flight condition at $\alpha_{(X=0)} \approx 10^{\circ}$.

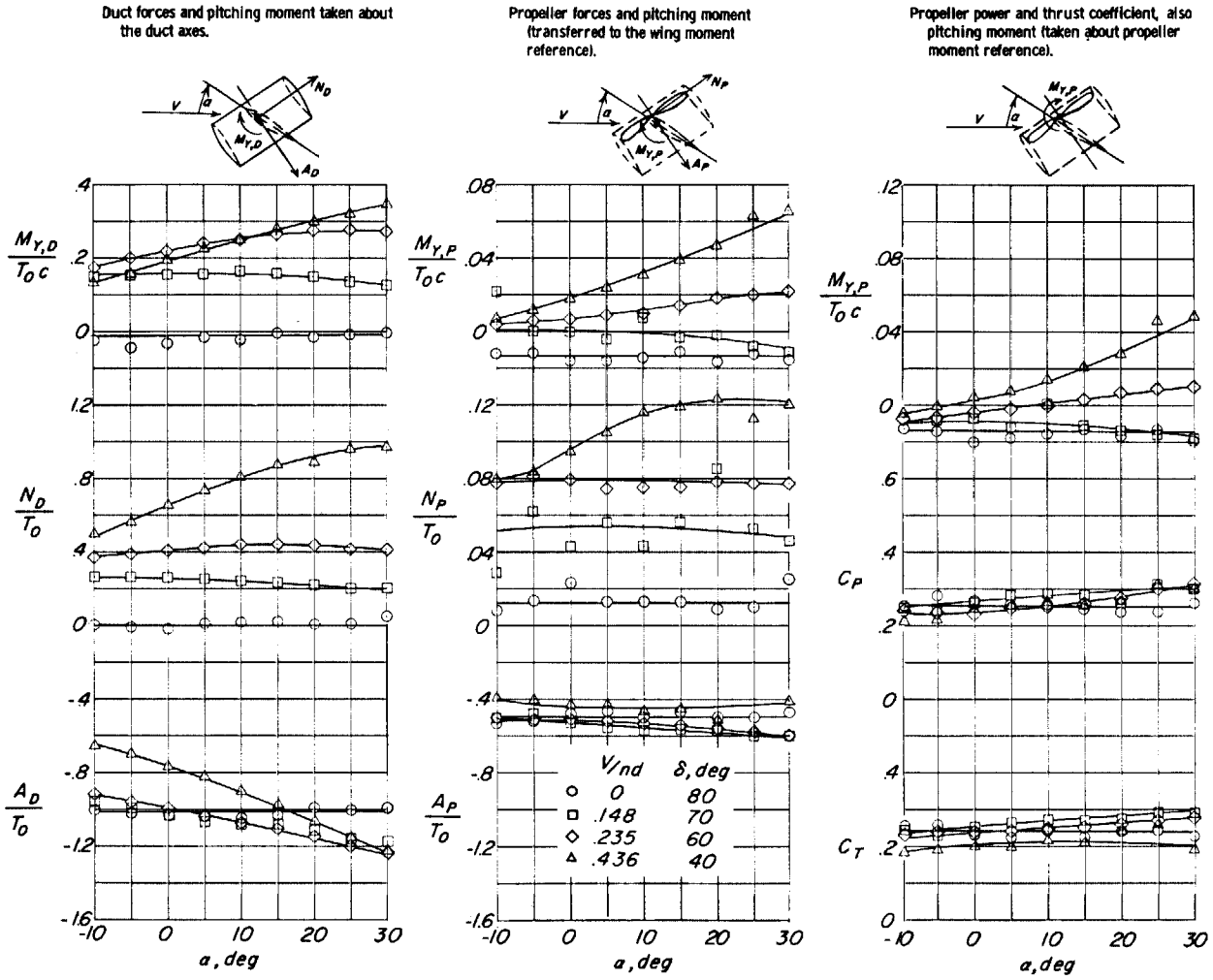

(d) (e) (f)

Figure 14.- Continued.

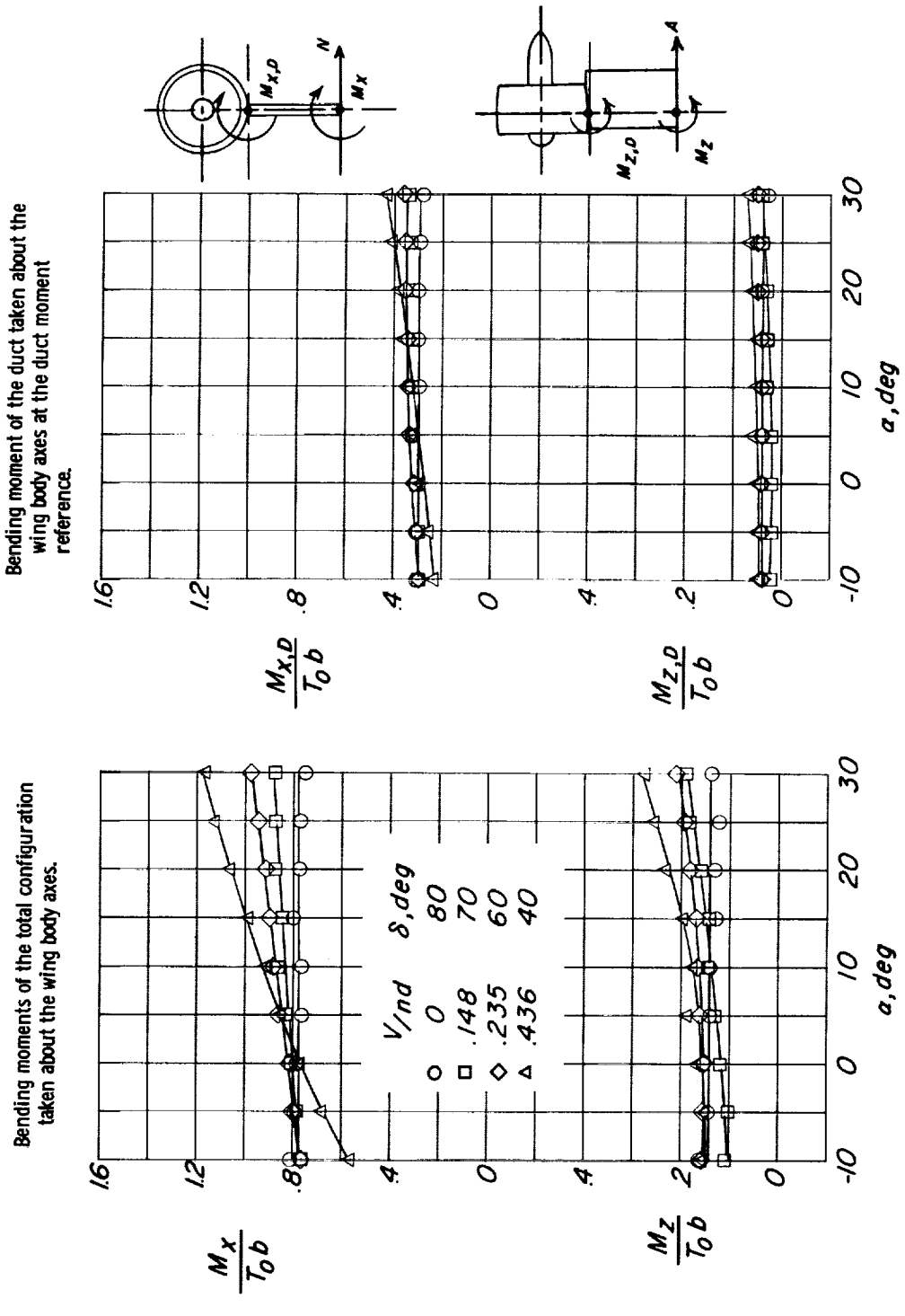

Figure 14.- Concluded.

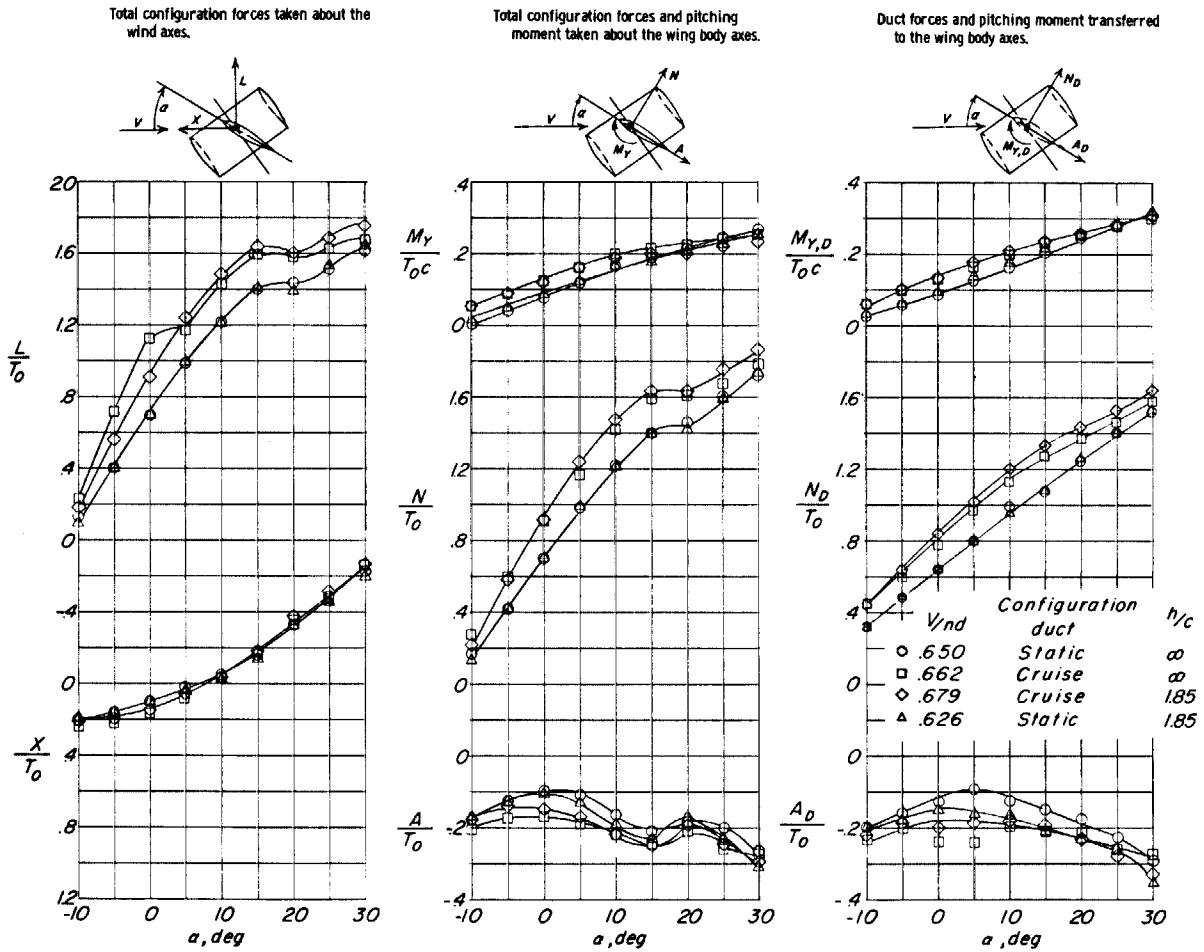

Figure 15.- Comparison of aerodynamic characteristics of static and cruise duct configurations out of ground effect with those for the same configurations in ground effect for a steady level flight condition at $\alpha_{(X=0)} \approx 10^{\circ}$. $\delta = 20^{\circ}$.

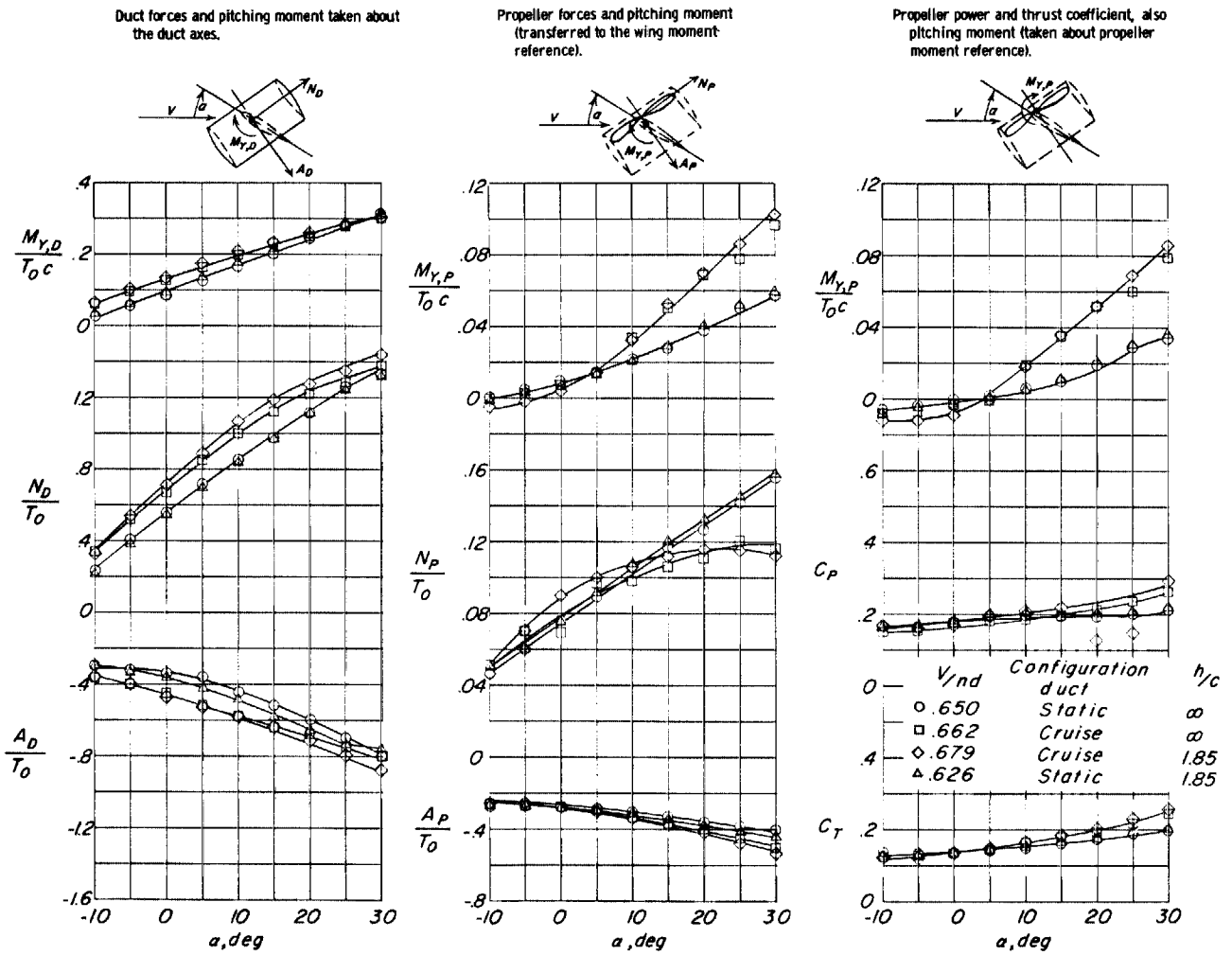

(d) (e) (f)

Figure 15.- Continued.

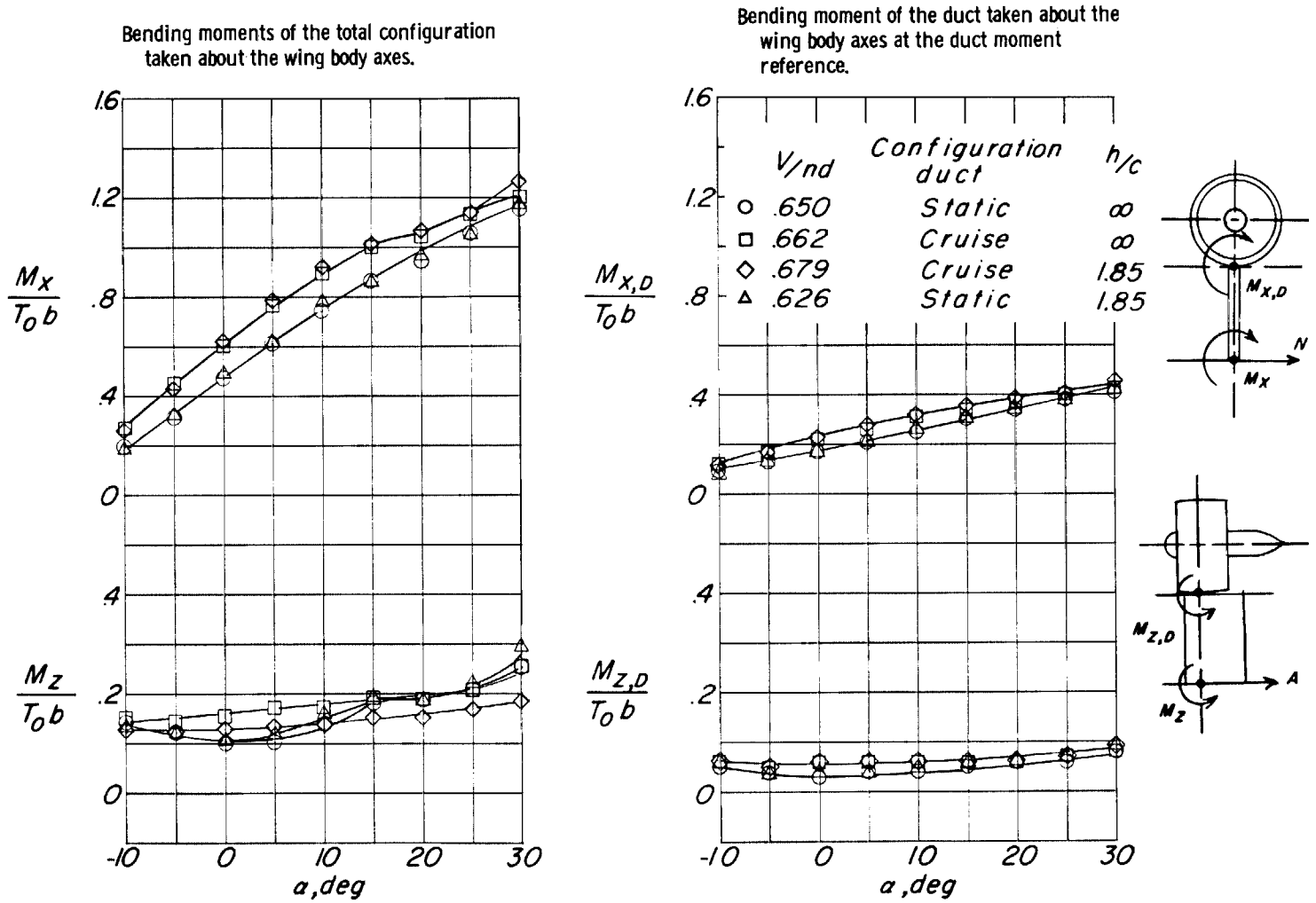

Figure 15.- Concluded.

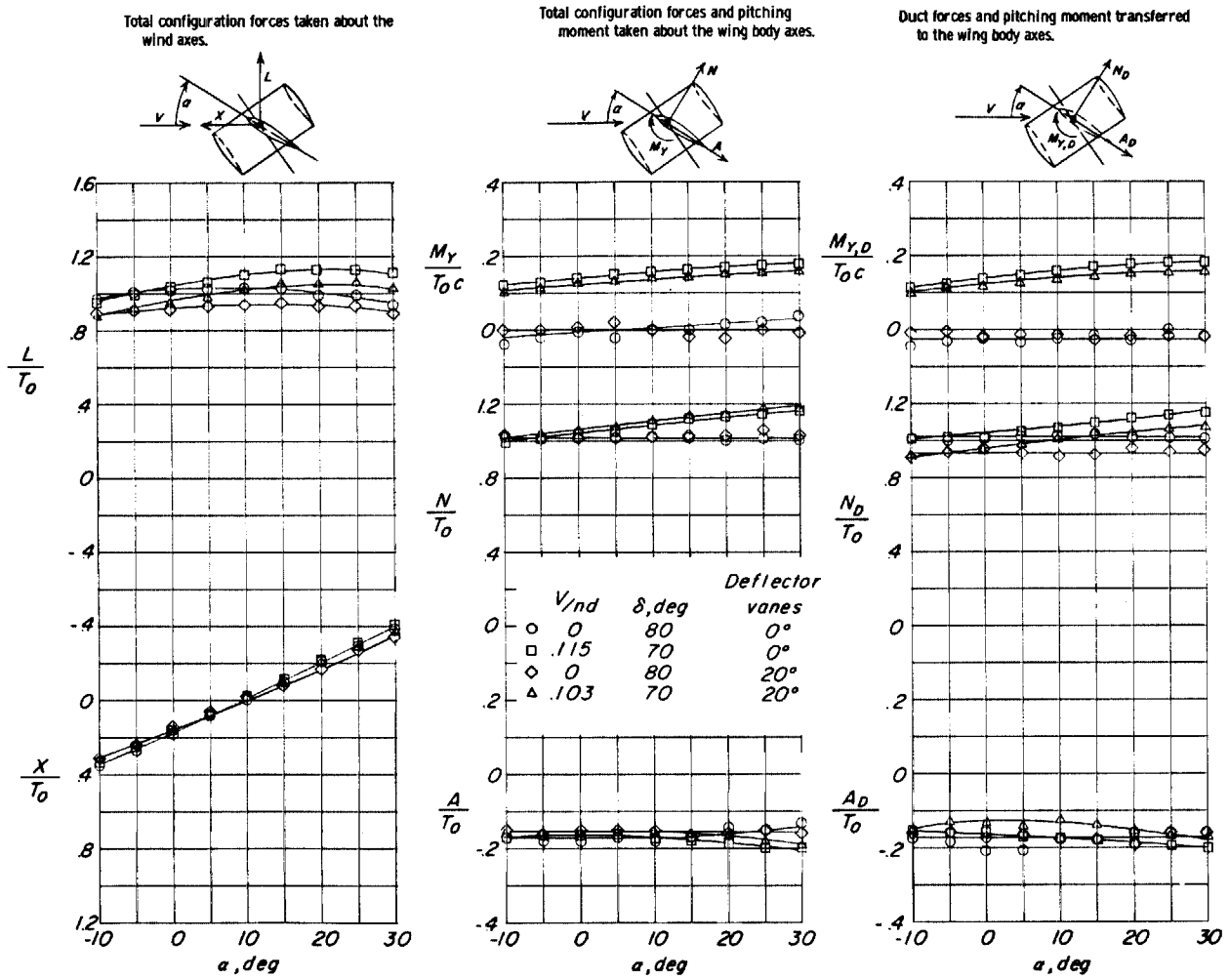

Figure 16.- Aerodynamic characteristics of static duct configuration with deflector vanes in rear of duct. Steady level flight at $\alpha \approx 10^{\circ}$; $h/c = \infty$.

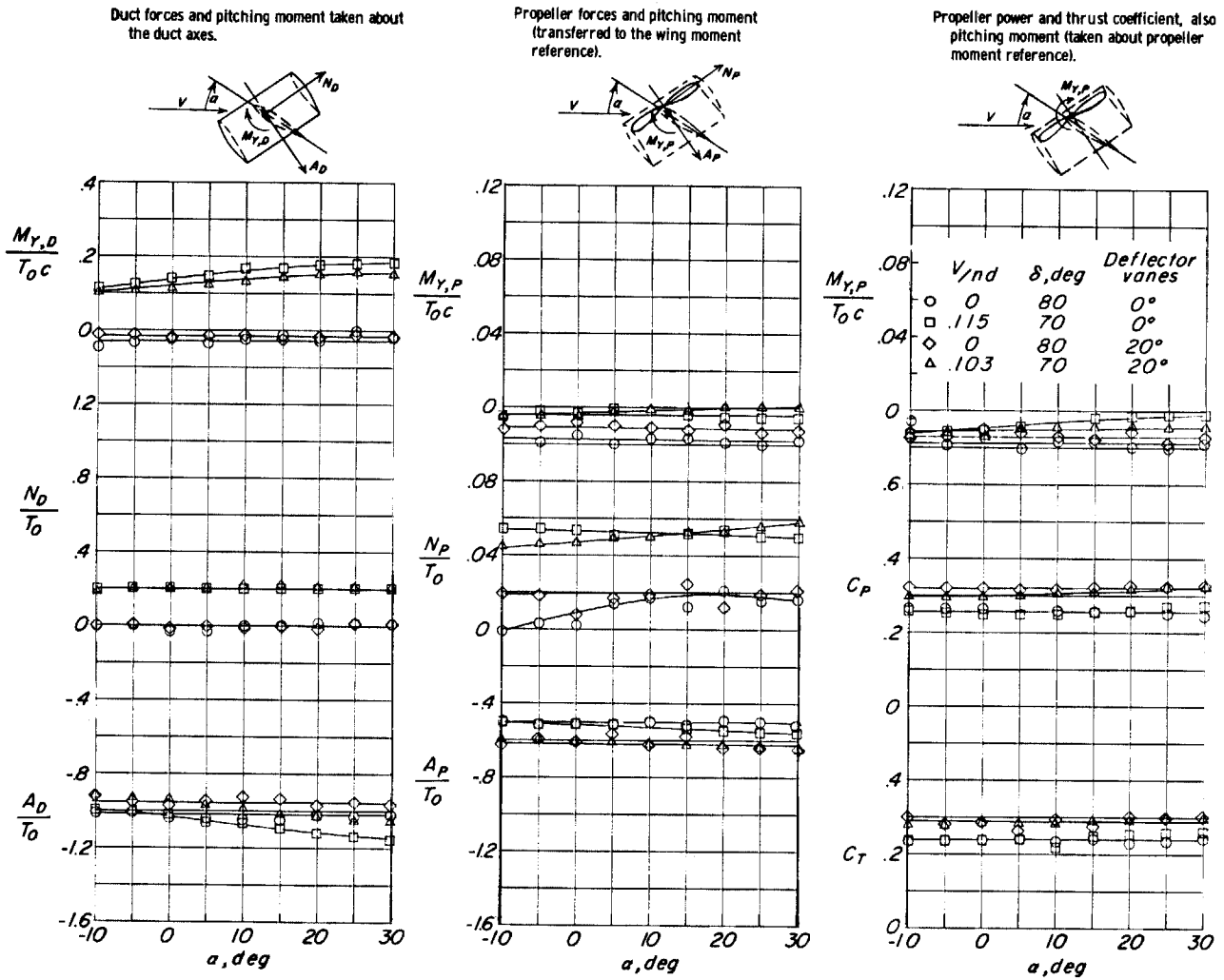

Figure 16.- Continued.

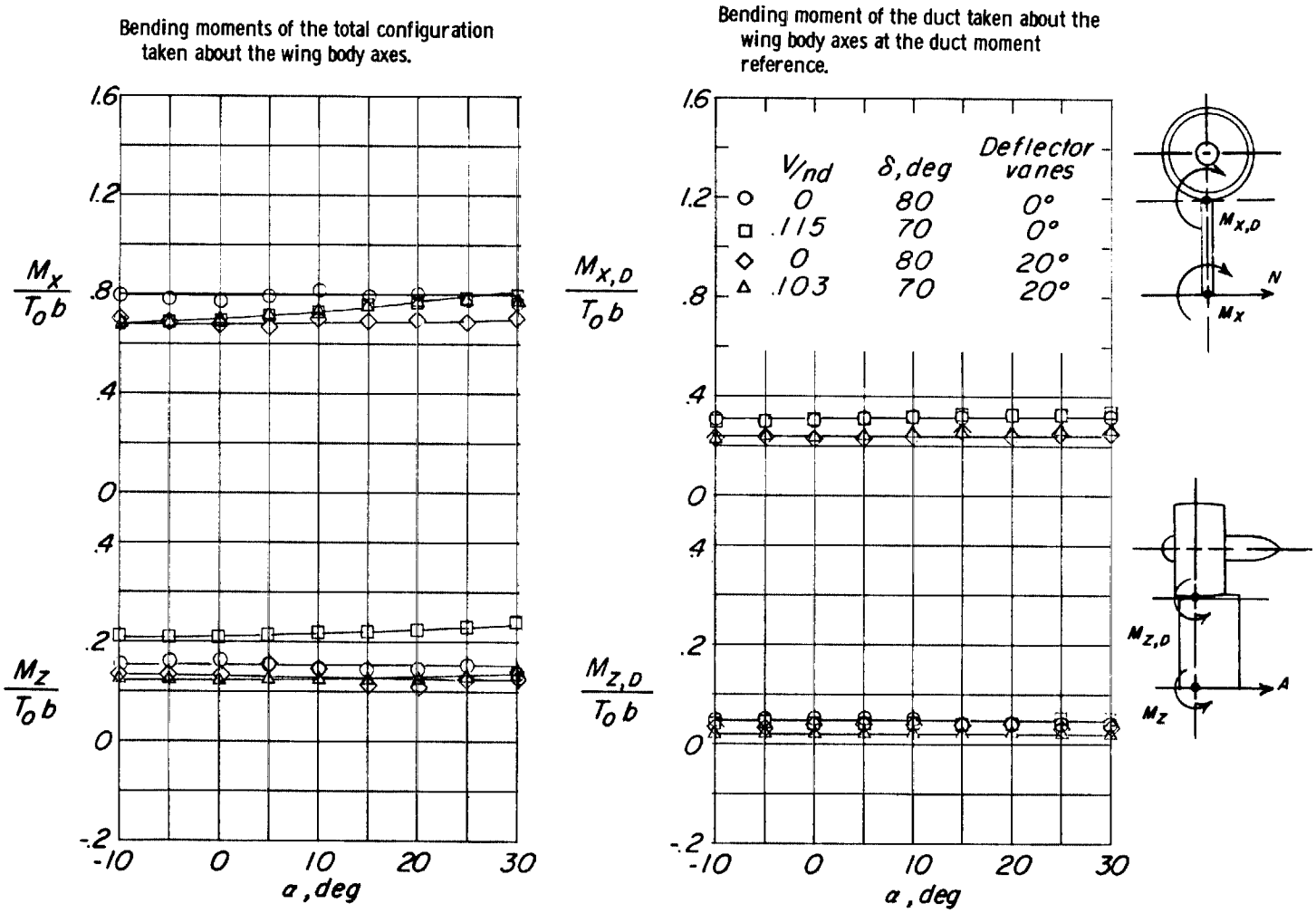

Figure 16.- Concluded.

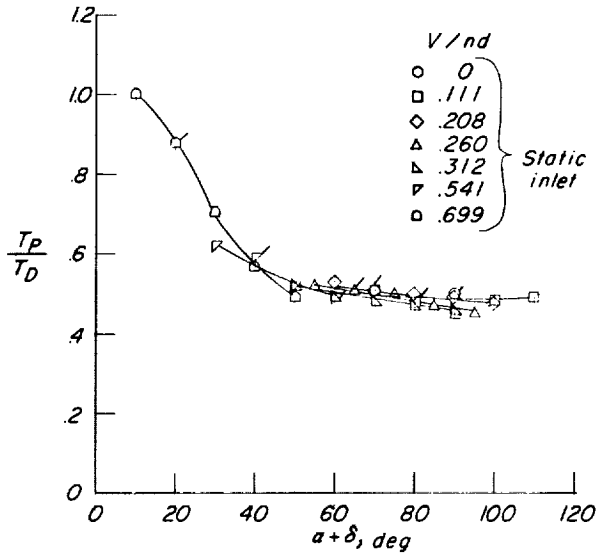

(a) Range of $\alpha + \delta$ for a number of advance ratios; condition of of steady level flight at $\alpha_{(X=0)} \approx 0^{\circ}$ indicated by flagged symbols.

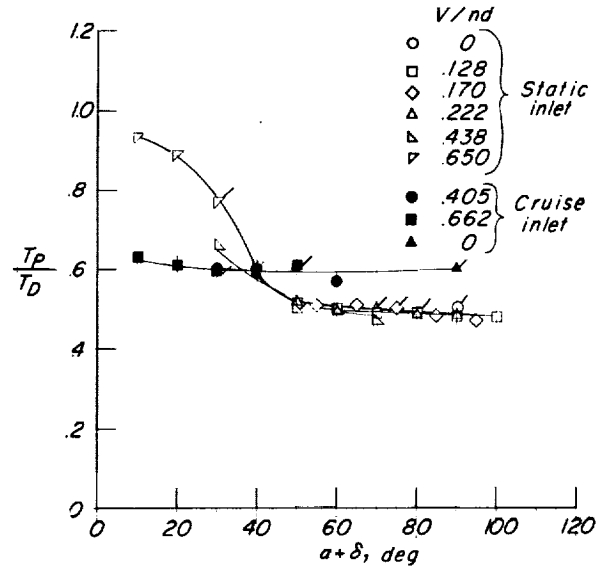

(b) Range of $\alpha + \delta$ for a number of advance ratios; conditions of steady level flight at $\alpha_{(X=0)} \approx 10^{\circ}$ indicated by flagged symbols.

Figure 17.- Division of thrust loads varied through an angle-of-attack range. $h/c = \infty$.

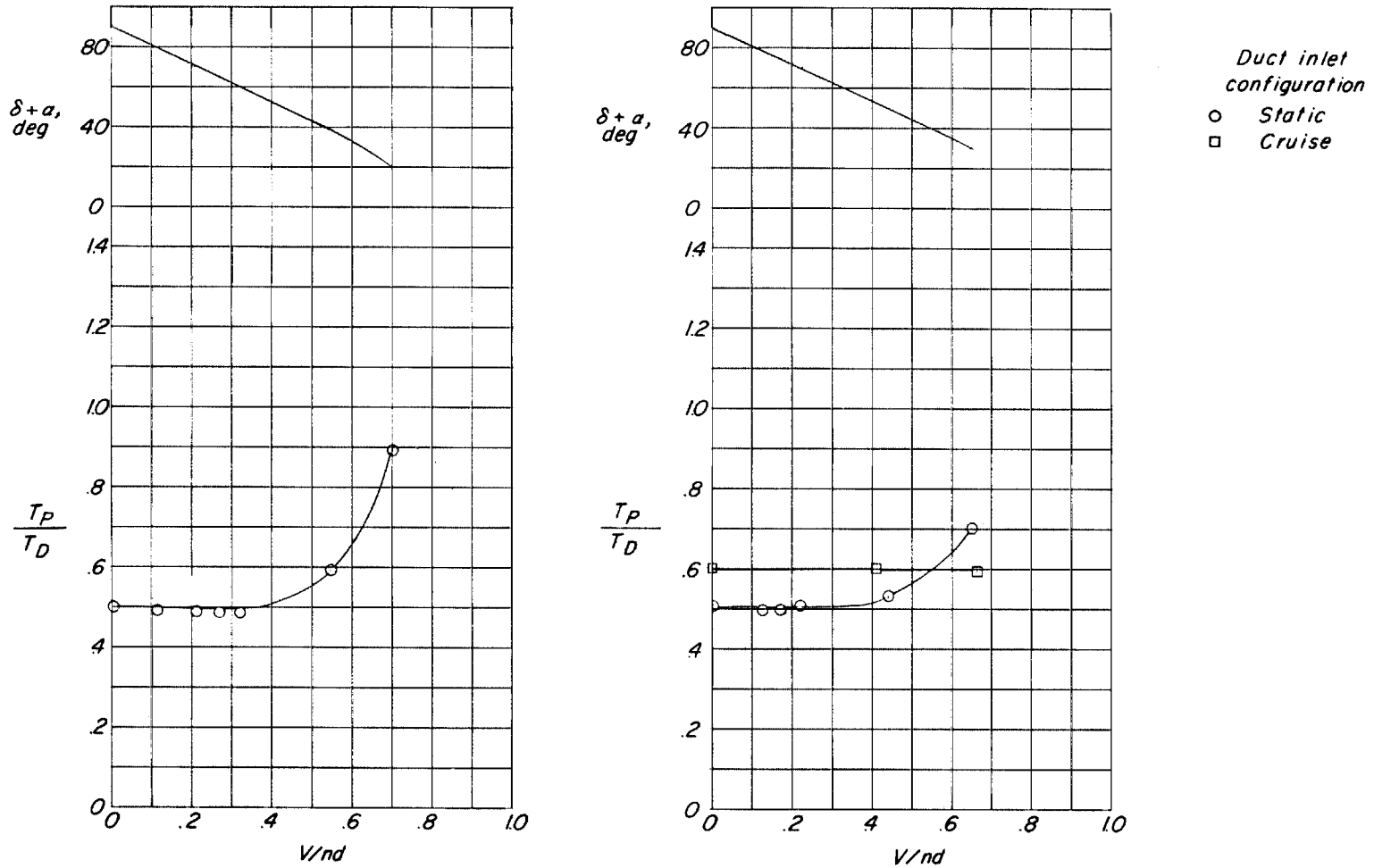

(a) $\alpha_{(X=0)} \approx 0^\circ$.

(b) $\alpha_{(X=0)} \approx 10^\circ$.

Figure 18.- Ratio of propeller thrust to total duct thrust for steady level flight. h/c = ∞.

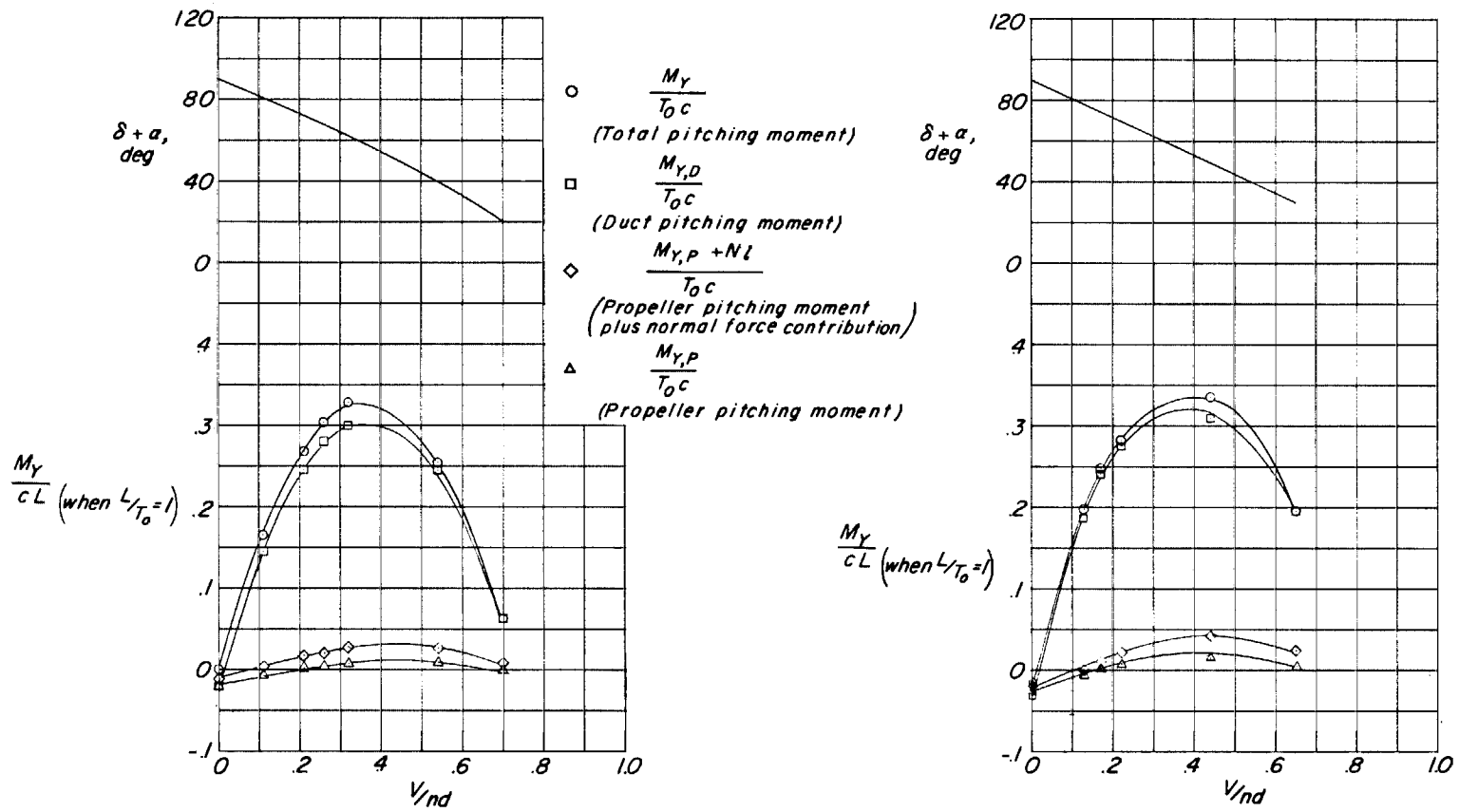

(a) $\alpha_{(X=0)} \approx 0^\circ$.

(b) $\alpha_{(X=0)} \approx 10^\circ$.

Figure 19.- Division of pitching-moment loads as a function of advance ratio. h/c = ∞; static duct; steady level flight.

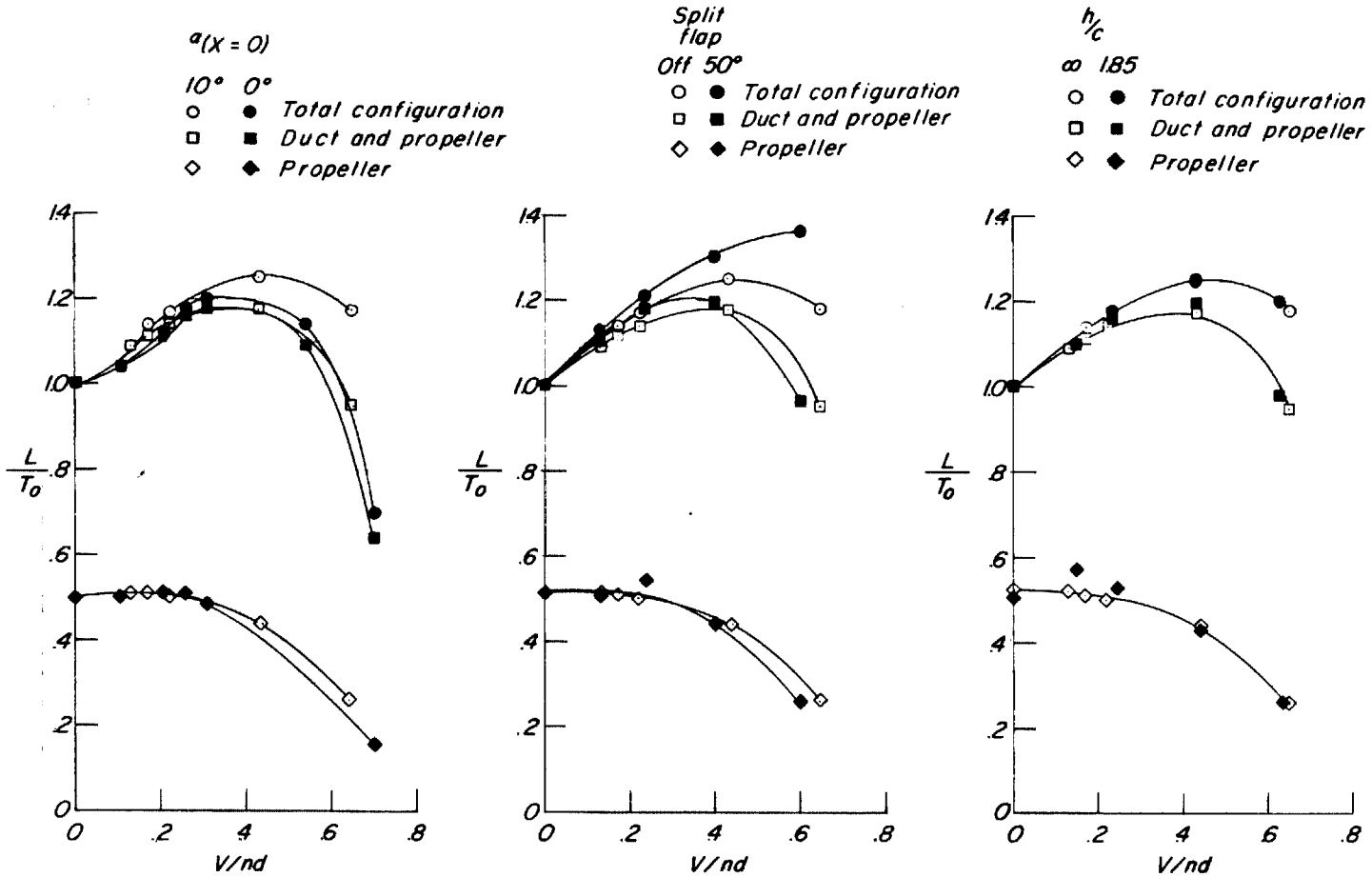

(a) Comparison of $\alpha_{(X=0)} \approx 10^{\circ}$ transition with $\alpha_{(X=0)} \approx 0^{\circ}$ transition.

(b) Flap effectiveness in transition. $\alpha_{(X=0)} \approx 10^{\circ}$.

(c) Ground effect. $\alpha_{(X=0)} \approx 10^{\circ}$.

Figure 20.- Division of lift loads presented as a function of advance ratio.

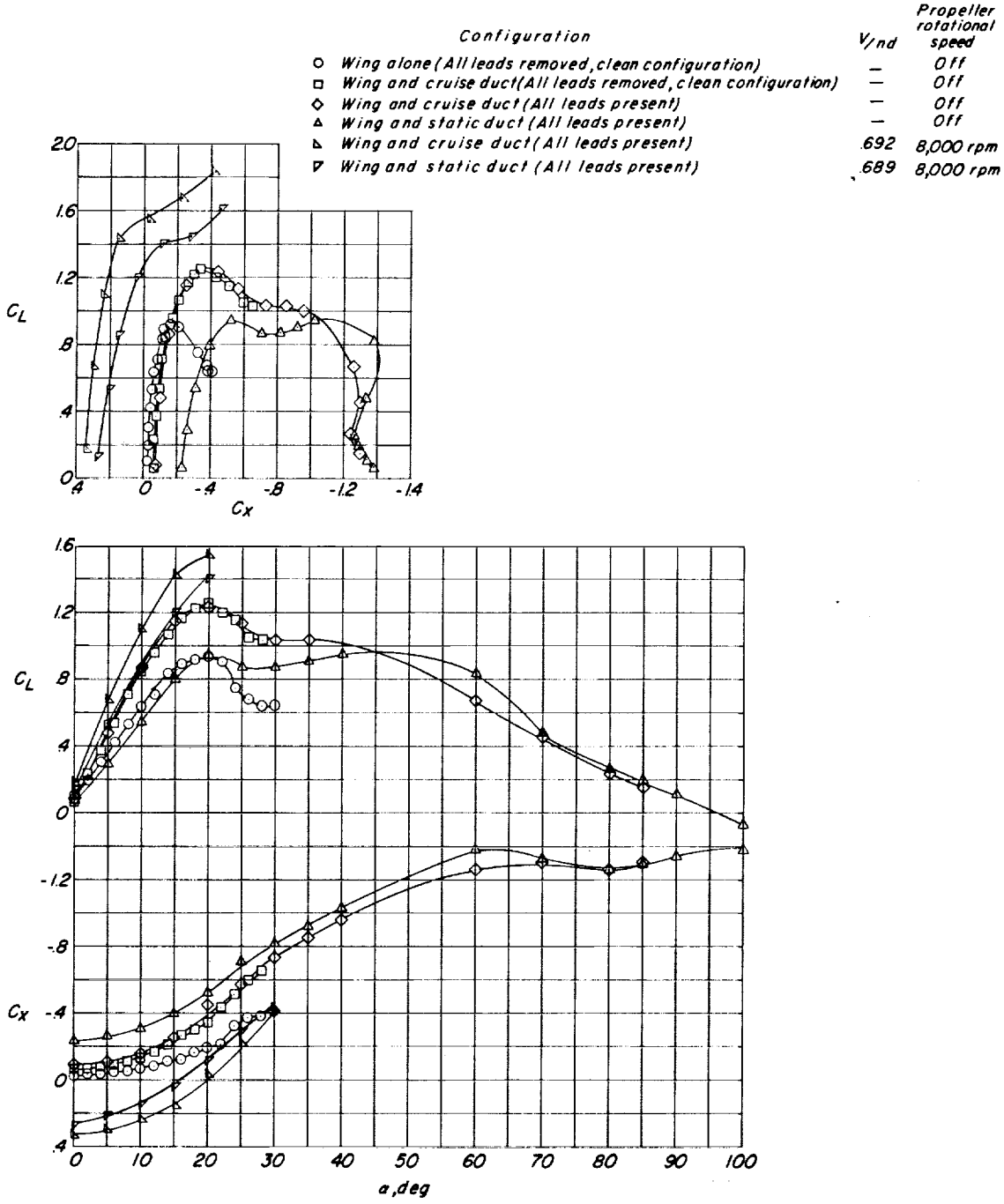

Figure 21.- High-speed aerodynamic characteristics of various configurations, power off and power on. (Data for wing and duct nondimensionalized on wing and duct planform area (3.7 square feet), data for wing alone nondimensionalized on wing area (2.0 square feet).) $\delta = 0^{\circ}$.

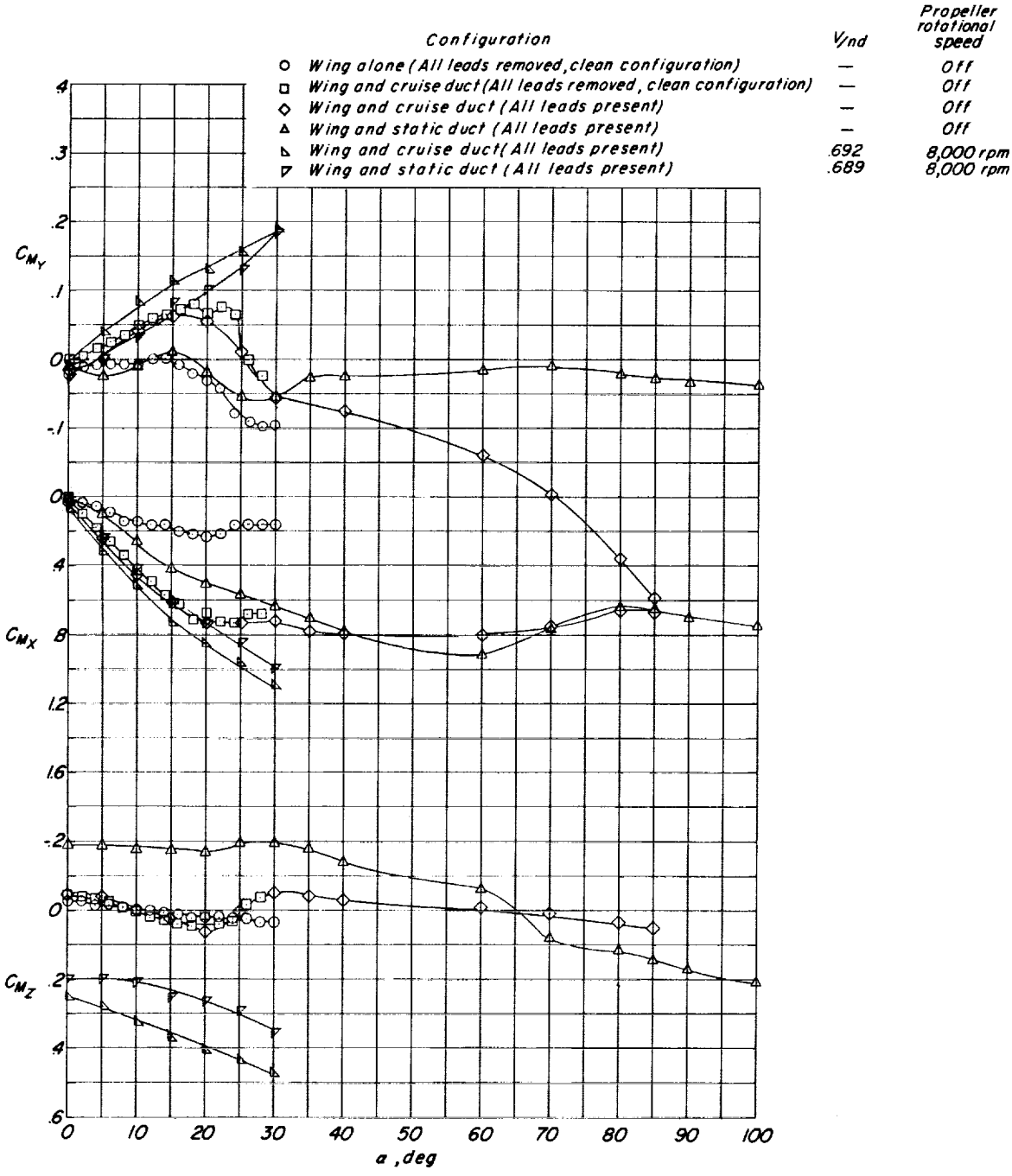

Figure 21.- Concluded.

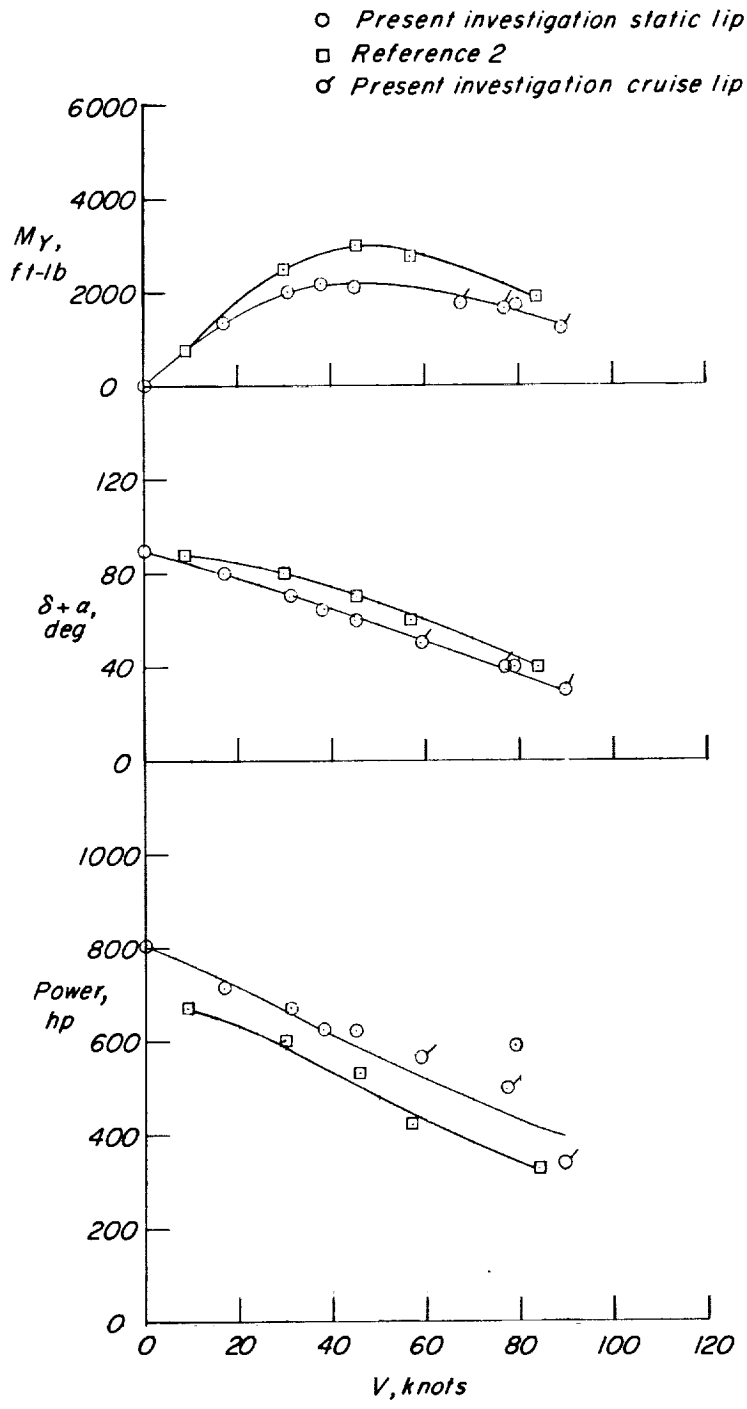

Figure 22.- Comparison of a steady level flight transition of the present investigation with reference 2 (assumed aircraft weight, 3,000 pounds; exit diameter, 54.05 inches).

NASA TN D-1257
National Aeronautics and Space Administration.
DIVISION OF AERODYNAMIC LOADS ON A SEMI-SPAN TILTING-DUCTED-PROPELLER MODEL IN HOVERING AND TRANSITION FLIGHT. Kalman J. Grunwald and Kenneth W. Goodson. May 1962. 57p. OTS price, $1.50.
(NASA TECHNICAL NOTE D-1257)

The investigation was conducted on a wing-tip-mounted ducted-propeller configuration through a duct-angle range (90° to 0°) and an advance-ratio range (0 to 0.699) to cover conditions of hovering flight and transition flight. Most of the normal-force and pitching-moment loads experienced by the configuration were carried by the duct at transition speeds. The propeller and wing contribution to the over-all normal force and pitching moment were small. The over-all lift of the configuration can be increased through the transition speed range by flying at a positive angle of attack and by the addition of some high-lift device such as a flap.

I. Grunwald, Kalman J.
II. Goodson, Kenneth W.
III. NASA TN D-1257

(Initial NASA distribution:
1, Aerodynamics, aircraft;
51, Stresses and loads.)

NASA

NASA TN D-1257
National Aeronautics and Space Administration.
DIVISION OF AERODYNAMIC LOADS ON A SEMI-SPAN TILTING-DUCTED-PROPELLER MODEL IN HOVERING AND TRANSITION FLIGHT. Kalman J. Grunwald and Kenneth W. Goodson. May 1962. 57p. OTS price, $1.50.
(NASA TECHNICAL NOTE D-1257)

The investigation was conducted on a wing-tip-mounted ducted-propeller configuration through a duct-angle range (90° to 0°) and an advance-ratio range (0 to 0.699) to cover conditions of hovering flight and transition flight. Most of the normal-force and pitching-moment loads experienced by the configuration were carried by the duct at transition speeds. The propeller and wing contribution to the over-all normal force and pitching moment were small. The over-all lift of the configuration can be increased through the transition speed range by flying at a positive angle of attack and by the addition of some high-lift device such as a flap.

I. Grunwald, Kalman J.
II. Goodson, Kenneth W.
III. NASA TN D-1257

(Initial NASA distribution:
1, Aerodynamics, aircraft;
51, Stresses and loads.)

NASA

NASA TN D-1257
National Aeronautics and Space Administration.
DIVISION OF AERODYNAMIC LOADS ON A SEMI-SPAN TILTING-DUCTED-PROPELLER MODEL IN HOVERING AND TRANSITION FLIGHT. Kalman J. Grunwald and Kenneth W. Goodson. May 1962. 57p. OTS price, $1.50.
(NASA TECHNICAL NOTE D-1257)

The investigation was conducted on a wing-tip-mounted ducted-propeller configuration through a duct-angle range (90° to 0°) and an advance-ratio range (0 to 0.699) to cover conditions of hovering flight and transition flight. Most of the normal-force and pitching-moment loads experienced by the configuration were carried by the duct at transition speeds. The propeller and wing contribution to the over-all normal force and pitching moment were small. The over-all lift of the configuration can be increased through the transition speed range by flying at a positive angle of attack and by the addition of some high-lift device such as a flap.

I. Grunwald, Kalman J.
II. Goodson, Kenneth W.
III. NASA TN D-1257

(Initial NASA distribution:
1, Aerodynamics, aircraft;
51, Stresses and loads.)

NASA

NASA TN D-1257
National Aeronautics and Space Administration.
DIVISION OF AERODYNAMIC LOADS ON A SEMI-SPAN TILTING-DUCTED-PROPELLER MODEL IN HOVERING AND TRANSITION FLIGHT. Kalman J. Grunwald and Kenneth W. Goodson. May 1962. 57p. OTS price, $1.50.
(NASA TECHNICAL NOTE D-1257)

The investigation was conducted on a wing-tip-mounted ducted-propeller configuration through a duct-angle range (90° to 0°) and an advance-ratio range (0 to 0.699) to cover conditions of hovering flight and transition flight. Most of the normal-force and pitching-moment loads experienced by the configuration were carried by the duct at transition speeds. The propeller and wing contribution to the over-all normal force and pitching moment were small. The over-all lift of the configuration can be increased through the transition speed range by flying at a positive angle of attack and by the addition of some high-lift device such as a flap.

I. Grunwald, Kalman J.
II. Goodson, Kenneth W.
III. NASA TN D-1257

(Initial NASA distribution:
1, Aerodynamics, aircraft;
51, Stresses and loads.)

NASA